Author correction

(Manuscript updated on 8 November 2024)

The initial published version of the article "Messager, G., Nivière, B., Lacan, P., Regard, V., & Blanc, E. (2024). Late Pleistocene activity and slip rates at the front of the Malargüe Fold-and-Thrust Belt (Southern Central Andes, Argentina). *τεκτονικα*, *2*(2), 52–84. https://doi.org/10.55575/tektonika2024.2.2.63" included a wrong version of Figure 18B. This issue happened during the manuscript production, when the lead author uploaded the figure files and mistakenly uploaded an old version of Figure 18. The correct figure was included in the version of the manuscript that was accepted by the reviewers and editors.

The incorrect figure depicted incremental displacements for successive terrace levels and highlighted potential displacement and age increments between Q4 and Q5 that could align with an average Pleistocene slip rate of 1.1 mm per year. In contrast, the updated version of Figure 18B accurately presents the age and cumulative shortening derived from a consistent rate of shortening that agrees with the earliest and latest estimated ages for Q4 (63-78 ka). The shaded area in this figure effectively illustrates the spectrum of plausible scenarios regarding the age and total shortening for Q5. While both versions of the figure convey similar findings, the revised one offers a more direct and comprehensible visual that agrees with the description provided in the figure caption and the main text of the paper.

TEKTONIKA

Late Pleistocene Fault Activity and Slip Rate in the Malarguë Fold-Thrust-Belt Front (Southern Central Andes, Argentina)

Grégoire Messager *[1,2], **Bertrand Nivière**[1], **Pierre Lacan**[3], **Vincent Regard**[4], **Eric Blanc**[5]

[1]Laboratoire des Fluides Complexes et de leurs Réservoirs - UMR5150-CNRS-TOTAL, Université de Pau et des pays de l'Adour, IPRA, BP 1155, F-64013 Pau Cedex, France | [2]Presently at: Equinor, G&G Research, Martin Linges vei 33, Fornebu, NO-1330 Fornebu, Norway | [3]Centro de Geociencias, Universidad Nacional Autónoma de México, Blvd. Juriquilla, 3001, 76230, Juriquilla, Querétaro, México | [4]Géosciences Environnement Toulouse (GET), Université de Toulouse, CNES, CNRS, IRD, UPS, (Toulouse) France, 14 avenue Edouard Belin, F-31400 Toulouse, France | [5]Equinor, G&G Research, Martin Linges vei 33, Fornebu, NO-1330 Fornebu, Norway

Abstract Hazardous faults in the retro-arc foreland of the southern Central Andes have predominantly been linked to the deformation of the Pampean flat-slab segment (28-33°S). There is a perceived decrease in Quaternary thrusting south of 33°S where the underlying subducted slab steepens. This is attributed to the limited documentation of the surface expression of thrusting in this region. Nevertheless, the Malargüe Fold-and-Thrust Belt (FTB; 34-36,30°S) in Argentina is subject to an intense seismic activity with historical earthquakes of magnitudes over 6. We report here evidence of Quaternary tectonic deformation to quantify the current slip rates along the Malargüe FTB thrust front. We have constructed a detailed morpho-structural map of the Sosneado thin-skinned thrust from extensive surface mapping and limited 2D seismic interpretation. The longitudinal profile of the alluvial deposits of the Atuel River reveals two 7 km-wide folds and associated growth strata at the front of the Malargüe FTB. Field investigations have led to the identification of several reverse faults dissecting Quaternary alluvial deposits. New Terrestrial Cosmogenic Nuclides dating of two alluvial terraces (71-75 ± 7 ka) assign their age of abandonment and, consequently, the deformation to the late Pleistocene. We use a simple shear analytical solution to estimate and quantify the cumulated deformation associated with the frontal thrust since the abandonment the alluvial terraces. Results indicate slip rates of about 1.0-1.3 ± 0.2 mm.yr^{-1} during the late Pleistocene. Structural restoration of the seismic cross section back to mid Miocene (9 Ma) suggests a later shortening of about 1500 m compatible with an average strain rate of only 0.16 mm.yr^{-1}. This suggests that the frontal thrust has been actively deforming during the Quaternary. By comparing the slip rates obtained from our study of the frontal Malargüe FTB with slip rates reported from the Pampean flat-slab zone, we suggest that the Malargüe FTB should be classified as a hazardous thrust system. Our findings indicate that the initial perception of a lack of active deformation and related hazards in the Andean retro-arc foreland related to slab steepness may be skewed.

Executive Editor:
Robin Lacassin
Associate Editor:
Jack Williams
Technical Editor:
Mohamed Gouiza

Reviewers:
Carlos Costa
Martine Simoes

Submitted:
9 August 2023
Accepted:
23 May 2024
Published:
2 September 2024

1 Introduction

In the San Juan and Mendoza provinces of Argentina in the southern Central Andes (27-35°S), intra-crustal seismic activity appears to coincide with retro-arc tectonic uplifts (Figure 1A; *Pardo et al.*, 2002), driven by the subduction of the Juan Fernández Ridge (28-33°S) and the Pampean flat-slab. This subduction configuration enhances plate coupling between the subducting Nazca plate and the overriding South American plate (Figure 1A; *Jordan et al.*, 1983; *Ramos et al.*, 2002; *Ramos and Kay*, 2006): numerous geophysical and field studies have been conducted to identify and characterize the kinematics of the seismogenic crustal faults in the region (*Kadinsky-Cade et al.*, 1985; *Costa and Finzi*, 1996; *Langer and Hartzell*, 1996; *Siame et al.*, 2002, 2015; *Brooks et al.*, 2003; *Alvarado et al.*, 2005; *Alvarado and Beck*, 2006; *Schmidt et al.*, 2011; *Rockwell et al.*, 2014, 2022; *Costa et al.*, 2019, 2021; *Rothis et al.*, 2019; *Oro et al.*, 2023). The distribution of earthquakes within the Andean Cordillera and its retro-arc foreland displays distinct patterns: for example, seismicity extends to the broken foreland (Sierras Pampeanas) of the San Juan area (SJ; 31-33°S), westwards along the crustal orogenic front (Precordillera) of the Mendoza area (Me; 33-34°30'S), and southwards

*✉ gmess@equinor.com

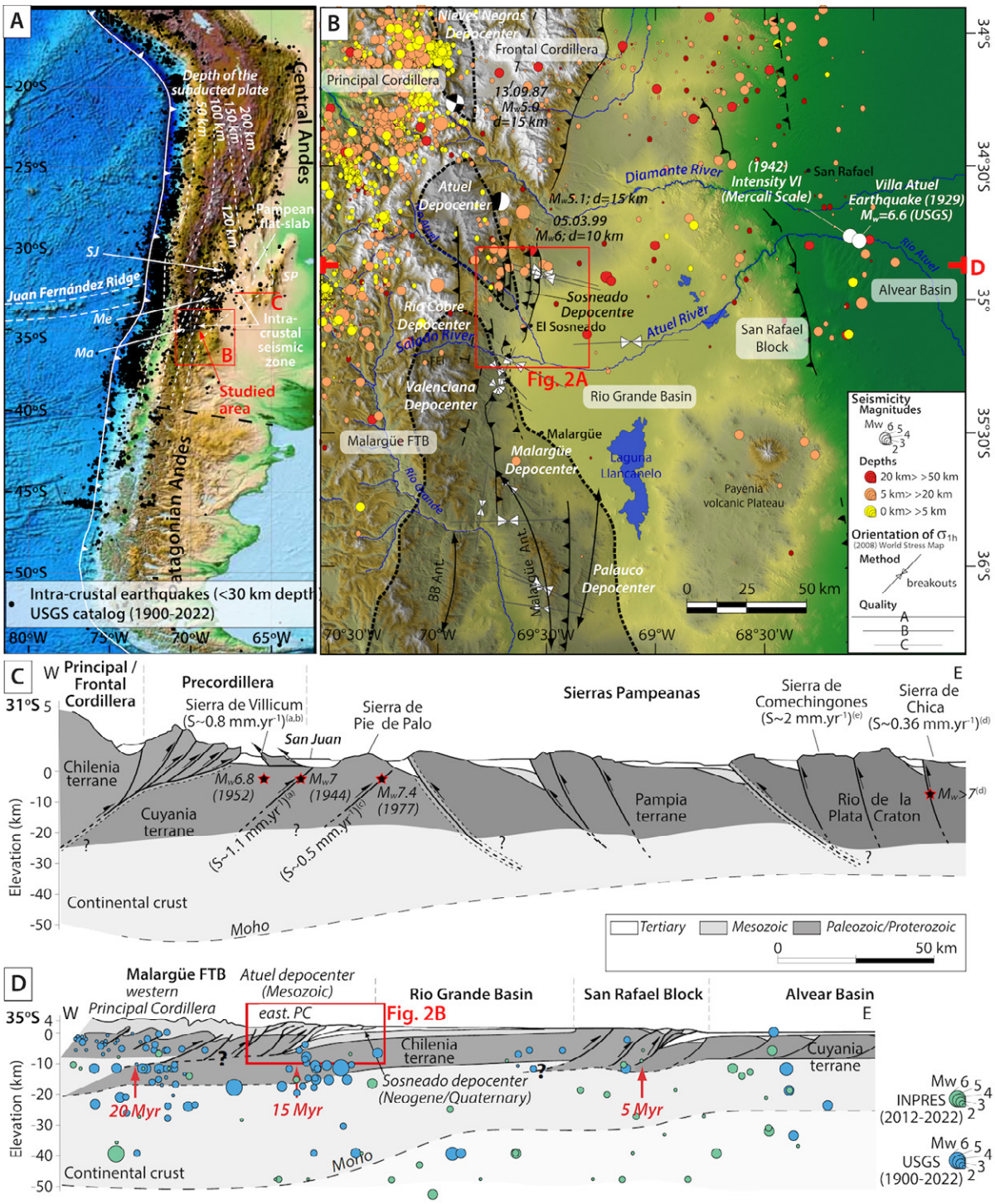

Figure 1 – **A-** Regional tectonic framework of the Pampean flat-slab and its induced intra-crustal seismicity; *SJ*: San Juan; *Me*: Mendoza; *Ma*: Malargüe; *SP*: Sierras Pampeanas. **B-** Tectonic setting of the Northern Neuquén Basin (located in A). The eastern border of the Malargüe FTB consists of deep-seated crustal faults and Mesozoic depocenters (grey areas) known respectively as, from south to north, the Palauco, Malargüe, Valenciano, Río Cobre, Atuel and Nieves Negras depocenters. Our study area focused on the eastern border of the Atuel Mesozoic depocenter where the Tertiary-Quaternary synorogenic deposits are laid (red rectangle). The maximum horizontal stress direction (σ_{Hmax}) is deduced from 14 wellbores reported in the World Stress Map (WSM) dataset (*Guzmán et al.*, 2007) with quality ranging from A (highest confidence) to C (lowest confidence) following WSM criteria. Earthquakes are from the USGS National Earthquake Centre catalogue compilation (CERESIS, NEIC, USGS) and from the Argentinean INPRES catalogue. **C-** Structural cross section in the Andean retroarc of the Pampean flat-slab region (31°S; located in A). The section displays the main tectonic domains and Pleistocene fault kinematics (Modified from *Ramos et al.*, 2002). Superscripts (a) to (e) refers to (a) *Rockwell et al.* (2014), (b) *Siame et al.* (2002), (c) *Siame et al.* (2015), (d) *Costa et al.* (2021) and (e) *Costa and Finzi* (1996). **D-** Structural cross-section of the eastern Malargüe FTB is modified from *Folguera et al.* (2009) (location on map in B). The earthquakes plotted on the section have their epicenters less than 12 km away from the section trace and their hypocentral depths are projected orthogonally relative to the section. The red arrows indicate the age of basement fault initiation and younging to the east (*Folguera et al.*, 2009). Dashed lines indicate uncertain depth geometries. BB Ant.: Bardas Blancas Anticline; FEI: El Infernillo Fault; east. PC: eastern Principal Cordillera.

within the Principal Cordillera in the Malargüe area (*Ma*; 34°30'-35°S) (Figure 1A and B).

Historical earthquakes in the Precordillera of the San Juan and Mendoza region, as well as in the Sierras Pampeanas, reached magnitudes of 6-7.5 (Jordan et al., 1983). These events nucleate on crustal faults with slip rates estimated in between 0.3 and 2 $mm.yr^{-1}$ (Figure 1C; Smalley et al., 1993; Costa and Vita-Finzi, 1996; Siame et al., 2002, 2015; Alvarado and Beck, 2006; Schmidt et al., 2011; Rockwell et al., 2014; 2022; Costa et al., 2019, 2021).

Quaternary active thrusting is perceived as significantly sparser south of 33°S where the subducted slab steepens up to 35° and where plate coupling decreases (*Jordan et al.*, 1983; *Costa et al.*, 2020; *Lopasso et al.*, 2024). This region hosts imbricated thick- and thin-skinned thrust systems deforming Mesozoic post-rift sediments and are commonly referred to as fold-and-thrust belts (FTB), such as the Malargüe FTB (34°30'S -36°30'S; *Kozlowski et al.*, 1993; *Manceda and Figueroa*, 1995; *Giambiagi et al.*, 2001; *Kraemer et al.*, 2011). In this structural context, crustal blocks deviate the maximum horizontal stress within the crust (*Messager et al.*, 2010) and nucleate earthquakes of low to moderate magnitude, extending as far south as 38°S (*Messager et al.*, 2023). Spatial correlations between seismogenic areas recorded in earthquake catalogues from INPRES, CERESIS, NEIC, and USGS and several crustal-scale thrusts in the southern Central Andes (*Costa et al.*, 2006; *Branellec et al.*, 2016a; *Gregori and Christiansen*, 2018; *Olivar et al.*, 2023), suggest that crustal seismogenic faults appear to indeed accommodate shortening in the Frontal Cordillera and the Sierras Pampeanas further north (Figure 1B and D).

At latitude 35°S, along the Malargüe FTB and across the retro-arc foreland, earthquakes of magnitude up to 6 have in fact been historically recorded (Figure 1B and D). For example, a massive earthquake hit the San Rafael region (southern Mendoza Province, Argentina) on May 30th, 1929. It even drew the attention of earthquake geologists all the way to the eastern border of the eponym basement block (Figure 1B and D; e.g., *Costa et al.*, 2006; *Folguera et al.*, 2015). However, the source faults of these events have received limited scrutiny, and to date there is no published kinematic analysis to quantify the associated deformations. In addition, limited understanding of structural mechanisms at play has prevented a thorough assessment of the seismogenic potential, and to date no surface breaks have been reported. The 1929 Villa Atuel earthquake, and another destructive earthquake that reached a VI intensity on the Mercalli scale on July 5th, 1942 (Figure 1B), has somewhat dwarfed the current strong persistent seismic activity further west along the Principal Cordillera (*Ma* in Figure 1B).

Along the eastern border of the Atuel Mesozoic rift depocenter inverted since the mid-Miocene, earthquakes of magnitude 5-6 are documented. These earthquakes lay along the crustal thrust front of the eastern Principal Cordillera of the Malargüe FTB (Figure 1B and D). This fits with recent reports of Pleistocene deformation in Cerro Pencal and Puesto Rojas (35°10'S), where Cretaceous sediments overthrust Quaternary deposits. *Mescua et al.* (2019) attribute this thin-skinned deformation to displacements on the Puchenque and Malargüe faults, thick-skinned faults at front of the central Malargüe FTB. *Colavitto et al.* (2019) also illustrate early Pleistocene (post 1.7 Ma) reverse faulting in the southern Malargüe FTB (36°40'S). Additionally, the profile of a mid-Quaternary (450 ka) strath terrace along the Diamante River, north of the Río Grande Basin, exhibits large wavelength folding (*Baker et al.*, 2009) interpreted as the result of a seismogenic, west-verging, blind crustal thrust along the western border of the San Rafael Block (34°30'S; *Olivar et al.*, 2023).

While the surface expression of active thrusts has been extensively studied in the provinces of Mendoza and San Juan, where seismic hazards are perceived as significant due to the underlying flat slab subduction, surface deformation in the Malargüe area has not been investigated as thoroughly. Quantitative analysis of the deformation in that area is either lacking or limited to the Miocene-Early Pleistocene strata (*Lopasso et al.*, 2024). Nonetheless, seismic activity in the Principal Cordillera is as significant as further north. In this study, we aim to quantify the deformation recorded in the Quaternary terraces along the thrust front of the northern Malargüe FTB (Figure 1B and D). Our focus lies on the El Sosneado area, where we observe folded alluvial terraces right above the thin-skinned frontal thrust, alongside evidence for surface ruptures (Figure 1B and D). Our study combines subsurface seismic interpretations with topographic analysis of satellite imagery, field observations complemented with cosmogenic nuclide dating of the terraces. By doing so, we aim to clarify the precise location of the fault sources driving active morphogenesis along the front of the Malargüe FTB. This allows us to better estimate slip rates along the thrust front of the Principal Cordillera and to discuss its hazardous nature.

2 Geological Setting

2.1 Regional Tectonic Framework

The pre-Andean geological history recorded various tectonic phases, establishing an enduring structural framework that shaped the evolution of the Andean orogeny and the current morphostructural variations along its strike (*Ramos*, 1994; *Charrier et al.*, 2007; *Nivière et al.*, 2013).

The accretion of allochthonous terrains along the western margin of the Gondwana supercontinent during the Precambrian and Paleozoic shaped the western margin of the South American plate (*von*

Gosen, 1998; *Ramos et al.*, 2000; *Charrier et al.*, 2007). The whole crust is dissected by NNW-SSE to NNE-SSW faults steeply dipping to the east and spanning up to more than 600 km (e.g., *Snyder et al.*, 1990; *Cominguez and Ramos*, 1991; *Regnier et al.*, 1992; *Zapata and Allmendinger*, 1996; *Astini*, 1998; *Gimenez et al.*, 2000; *Chernicoff and Zappettini*, 2004). In the southern Central Andes, from west to east these terrains are respectively the Río de la Plata, the Pampia, the Cuyania, and the Chilenia cratons (Figure 1C *Ramos*, 1988; *Ramos et al.*, 1996).

The collapse of the Paleozoic Gondwana orogen during the Triassic and the early Jurassic occurred in a broad intracontinental extensional regime, in the form of NW–SE-oriented grabens and half-grabens (*Uliana et al.*, 1989; *Vergani et al.*, 1995; *Franzese and Spalletti*, 2001). This extensional regime was influenced by Proterozoic and Paleozoic discontinuities (*Ramos*, 1994). These Mesozoic extensional depocenters seeded the Neuquén Basin within the Chilenia terrane (40°-34°30'S), the Cuyo Basin (35°30'-32°S) within the Cuyania terrane, and rifted basins within the Río de La Plata and Pampia terranes (e.g., *Ramos et al.*, 2002).

The onset of the opening of the Atlantic Ocean in the late Cretaceous coincides with the initiation of the Andean orogeny (*Groeber*, 1929; *Ramos*, 1994; *Charrier et al.*, 2007). The rates of shortening in the foreland reflect the variations of plates relative velocities and convergence, impacting the geometry of the subducted slab and the degrees of coupling between the plates (*Steinmann*, 1929; *Pardo-Casas and Molnar*, 1987; *Ramos*, 1988; *Cobbold and Rossello*, 2003). The Andean orogeny went through three successive compressive phases: a first one during the Mid-Cretaceous and Paleocene (*Soler and Bonhomme*, 1990; *Cobbold and Rossello*, 2003; *Ramos and Kay*, 2006; *Rojas Vera et al.*, 2015), a second one during the Late Eocene (*Pardo-Casas and Molnar*, 1987; *Somoza*, 1998), and a third one during the early Miocene and the Plio-Pleistocene (*Cande and Leslie*, 1986; *Pardo-Casas and Molnar*, 1987; *Silvestro et al.*, 2005; *Cobbold and Rossello*, 2003; *Messager et al.*, 2010; *Huyghe et al.*, 2015; *Rojas Vera et al.*, 2015). These three phases are bounded by two quieter periods decrease in tectonic shortening intensity during the Oligocene-early Miocene and since the Pliocene (*Kay et al.*, 2006; *Folguera et al.*, 2009), during which the Andean volcanic arc migrated westwards and the subducted slab steepened. During the last 8-10 Ma, the subduction of the Juan Fernández Ridge triggered plate coupling and retro-arc uplifts in between 30°S and 33°S (Figure 1A *Allmendinger et al.*, 1990; *Ramos et al.*, 2002; *Anderson et al.*, 2007; *Martinod et al.*, 2010), maintaining flat slab geometries and intense tectonics after the Miocene. South of 33°S, a more steeply dipping slab marked a reduction in tectonic shortening and uplifts (*Folguera et al.*, 2009; *Galland et al.*, 2007; *Messager et al.*, 2010; *Huyghe et al.*, 2015; *Messager et al.*, 2023) during the Pliocene and Quaternary.

The present-day configuration of the southern Central Andes (27-40°S) in Argentina is largely influenced by structural inheritance (Figure 1C-D). East-verging crustal thrusts in the Principal and Frontal Cordilleras are controlled by the inversion of Mesozoic basins developed within the Chilenia terrane, contributing to the formation of the primary orogenic topography. Specifically, the Malargüe Fold-and-Thrust Belt (34°30'S – 36°30'S) inverts the northern and narrowest section of the Neuquén Basin (Figure 1B) whilst the San Rafael Block (35°S), the Precordillera, and the westernmost Sierras Pampeanas invert the Cuyo Basin in the Cuyania terrane (Figure 1C-D). The Sierras Pampeanas break the foreland up to 800 km away from the subduction trench by inverting the Mesozoic rifted basins and the Proterozoic suture zones of the Pampia and Río de la Plata terranes (Figure 1C). South of latitude 34°30'S, the narrow thrust belts of the Frontal Cordillera and Precordillera disappear, along with the narrowing broken foreland (*Jordan et al.*, 1983). This appears to be linked to variations in the basement configuration (Figure 1C-D).

Evidences for inversion of inherited structures and crustal thickening can be observed throughout the southern Central Andes and are tied to in- or out-of-sequence uplifts of crustal-scale blocks and the individualization of intramontaneous basins, following the dynamics of broken forelands (*Dávila and Astini*, 2003; *Hilley and Strecker*, 2005; *Strecker et al.*, 2012; *Dávila et al.*, 2012; *del Papa et al.*, 2013; *Huyghe et al.*, 2015; *García Morabito et al.*, 2021; *Messager et al.*, 2023). The localization of deformation largely depends on crustal thickness and fault strength to sustain topography, and the spatio-temporal distribution of crustal uplifts and erosion, the latter being influenced by climatic factors (*Hilley and Strecker*, 2005; *Hain et al.*, 2011). The noticeable morphostructural differences in the southern Central Andes at 34°30'S result from the complex interactions in between the inherited basement structures and the changes in regional shortening intensity, as well as the climate conditions over time (*Messager et al.*, 2023).

The distribution of active thrusts and earthquake epicenters is governed by the dynamics of a broken foreland; this implies that the active thrusts of the southern Central Andes are not necessarily solely accommodated along the orogenic thrust front but over the entire Argentinean Andes and their broken forelands (*Bande et al.*, 2020), where the potential for seismic activity extends during the Quaternary.

2.2 Morphostructural Settings of the Malargüe FTB

The Mesozoic Neuquén Basin extends to the west over the Principal Cordillera in Chile and to the east, as far as the Río Grande Basin. The northern segment of the Neuquén Basin is subdivided into five Mesozoic depocenters: Palauco, Malargüe, Valenciana, Río

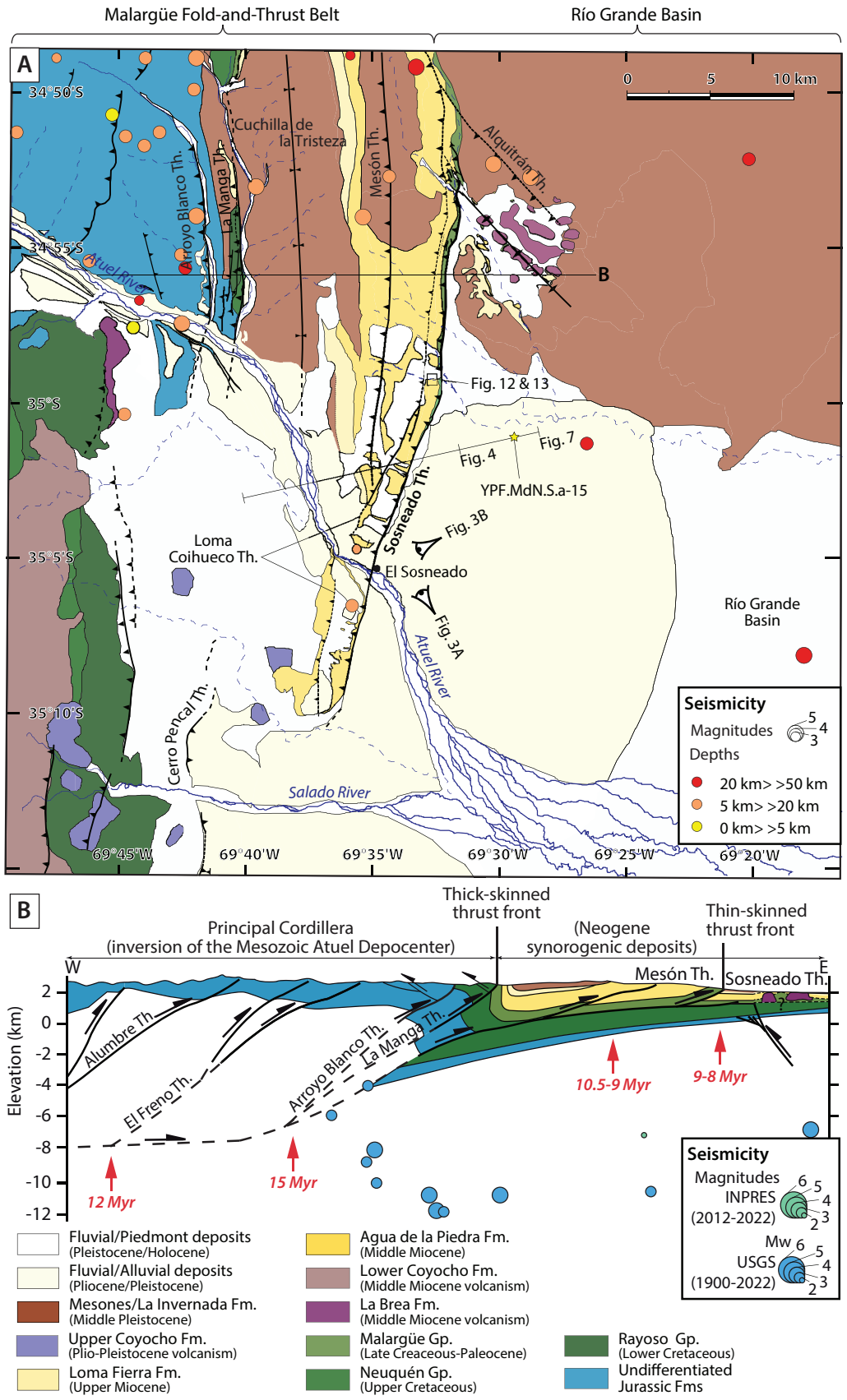

Figure 2 – A- Geological map of the northeastern Malargüe FTB, around the El Sosneado locality (after *Nullo et al.*, 2004; *Sruoga et al.*, 2005; *Giambiagi et al.*, 2008, new observations on Quickbird images). The yellow star refers to the location of the YPF well YPF.MdN.S.a-15. **B-** Structural cross section of the eastern Malargüe FTB (located in A; modified from *Giambiagi et al.*, 2008; *López Ordines et al.*, 2022; *Galland et al.*, 2024): the Arroyo Blanco and La Manga thrusts are the thick-skinned front of the Principal Cordillera, uplifting the Mesozoic Atuel Depocenter. The Mesón and Sosneado Thrusts are the thin-skinned thrust front of the Malargüe FTB, exhuming the Neogene synorogenic deposits. The red arrows indicate the age of basement fault initiation (*Giambiagi et al.*, 2008).

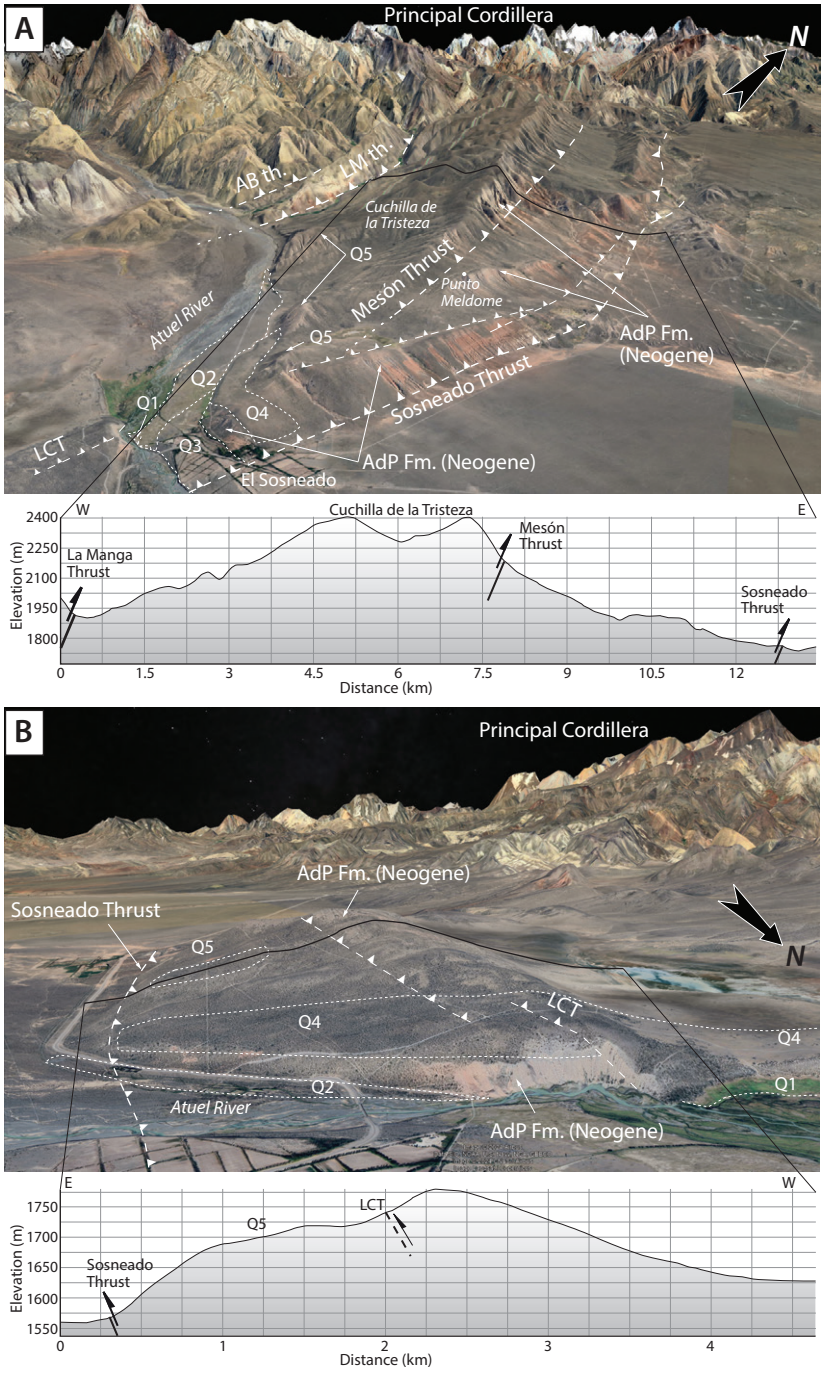

Figure 3 – Perspective views of the thrust front of the Malargüe FTB, north (A) and south (B) of the Atuel River, incorporating a topographic section across the frontal ridge. These images have been extracted from Google Earth. AB th.: Arroyo Blanco Thrust; LM th. : La Manga Thrust; LCT: Loma Coihueco Thrust; AdP: Agua de la Piedra Fm.. Q1 to Q5 refer to the five levels of alluvial surfaces of the Atuel River. The perspective viewpoints are shown by the eyes on Figure 2A.

Cobre, and Atuel (*Manceda and Figueroa*, 1995, Figure 1B) which were inverted during the late Cretaceous, ultimately leading to the growth of the Malargüe FTB (*Giambiagi et al.*, 2008). The f.t.b. is segmented by two distinct NW-SE striking Mesozoic depocenters, on the southeastern and northeastern borders of the Atuel and Valenciana depocenters (Figure 1B). Locally there is evidence for thin-skinned deformation linked to basement thrust propagation into the sedimentary cover (*Kozlowski et al.*, 1993; *Manceda and Figueroa*, 1995; *Mescua et al.*, 2014, 2019; *Branellec et al.*, 2016b). The Atuel Mesozoic depocenter is inverted through a set of west-dipping crustal thrusts, such as from west to east, the Alumbre, El Freno, and Arroyo Blanco thrust faults (Figure 2; *Kozlowski et al.*, 1993; *Manceda and Figueroa*, 1995; *Lanes*, 2005; *Giambiagi et al.*, 2008), and the thin-skinned east-verging Mesón, Sosneado, and Alquitrán thrust faults (*Giambiagi et al.*, 2008; *Bechis et al.*, 2010). The Mesón Thrust is marked by a 500 m-high scarp tapering southward and disappearing north of the Atuel River (Figure 3A). The Sosneado Thrust is exposed and lines a 100 m to 200 m-high ridge over 40-km distance striking NNE-SSW south of the Punto Meldome, and N-S until the Diamante River (Figures 1B and 3). Along the hanging wall

scarp, Neogene syn-orogenic deposits and Upper Cretaceous/Paleocene red sandstone and shale of the Malargüe Group are exposed (Figure 2). The Alquitrán blind thrust is deduced from the folding of the Paleogene to Pliocene strata (*Giambiagi et al.*, 2008) and west-verging basement faults (Figure 2 *López Ordines et al.*, 2022).

To the east, the Río Grande Basin forms a vast plain spanning 80 km from west to east and 100 km from north to south, at a regional elevation of approximately 1350 m (34°30'-36°30'S, Figure 1; *Silvestro et al.*, 2005; *Ramos and Kay*, 2006). The basin is filled up to 2000 m-thick Tertiary syn-orogenic sequences and resulting from the uplift and erosion of both the Principal Cordillera and the San Rafael Block. The San Rafael Block stands 150 m above the Río Grande Basin and 1000 m above the current foreland basin to the east. It is approximately 30-50 km wide and bounded to the north by west- and east-verging thick-skinned thrusts, NW-SE trending in the north and N-S trending in the south (*González-Díaz*, 1964; *Volkheimer*, 1978; *Kay et al.*, 1989; *Olivar et al.*, 2023).

The Salado and Atuel rivers currently drain the Río Grande Basin; they flow to the southeast across the Principal Cordillera and to the ENE over the Malargüe and the San Rafael Block (Figure 1). The western side of the Río Grande Basin is riddled with broad alluvial fans whilst its eastern border is dominated by lacustrine sediments (Figure 2). The rivers converge toward a single 300 m-deep narrow canyon cutting through the San Rafael Block and then merge with the Diamante River to flow southward along the western border of the Andean forebulge (Figure 1; *Nivière et al.*, 2013). Rivers in the Principal Cordillera are narrow (<200 m) and deeply incised (1500-2000 m) in contrast with those in the Río Grande Basin, anastomosed and meandering, with no evidence for incision or strong lateral migration. The catchment areas of the Diamante and Atuel rivers are approximately 2300-2500 km^2 each.

2.3 Neogene to Quaternary Propagation of the Orogenic Front

In this segment of the Andes, deformation propagates in sequence from west to east during the Late Cretaceous. The Río Cobre Mesozoic depocenter was exhumed and the eastern border of the Las Lenas High was uplifted (Figure 1B; e.g., *Mescua et al.*, 2014; *Branellec et al.*, 2016b). The La Valenciana Mesozoic depocenter was then located in the foreland basin right until the early Miocene when the deformation migrated to the east and the Malargüe anticline (*Jordan et al.*, 1983; *Ramos et al.*, 1996; *Giambiagi et al.*, 2001, 2008; *Bande et al.*, 2020). Synorogenic deposition was initially restricted to the area of the Mesozoic Malargüe Depocenter (*Silvestro et al.*, 2005), and the western part of the Mesozoic depocenter of La Valenciana formed a piggy-back basin, and by the late Miocene the Río Grande basin became the primary depositional area (*Silvestro et al.*, 2005).

Late Miocene and Pliocene synorogenic deposits of the Agua de la Piedra, Loma Fierra and Río Diamante formations document tectonic exhumation in the Principal Cordillera, in the Río Cobre Mesozoic depocenter, and along the eastern borders of the La Valenciana and Atuel Mesozoic depocenters (*Giambiagi et al.*, 2008; *Mescua et al.*, 2019; *Bande et al.*, 2020). Meanwhile, active deformation began to localize further east in the San Rafael Block (*Soria*, 1984; *Ramos and Kay*, 2006). The Tertiary exhumation of the Atuel Mesozoic depocenter was driven by an out-of-sequence inversion of thick-skinned Mesozoic faults over the last 20-15 Ma, and more recently by in-sequence thin-skinned deformation, i.e., the Mesón Thrust (10.5-9 Ma), the Sosneado and the Alquitrán thrusts (9-8 Ma) (Figure 2B *Giambiagi et al.*, 2008; *Bande et al.*, 2020).

The eastern border of the Atuel depocenter experiences a higher frequency of earthquakes with magnitudes ranging from 4 to 6, in comparison to the Western Cordillera where earthquakes of magnitude 4 or less occur within the first 10 km-depth, and the San Rafael Block where higher magnitudes of 4 and 5 are found in the eastern foreland (Figures 1 and 2). Focal mechanisms reveal a transpressive activity in the Principal Cordillera (Mw 5.9, 1987; Mw 6.5, 2004) and a compressive activity northwest of the Sosneado Thrust (Mw 5.8, 1999; *Alvarado et al.*, 2005, Figure 1B). Destructive earthquakes have been observed in the eastern border of the San Rafael Block in Las Malvinas (1861 and 1929), in San Carlos (1861), and General Alvear (1913) cities (Figure 1B). The Las Malvinas-Vila Atuel earthquake (1929) and ongoing faults of the area (Aisol, Valle Grande, Las Malvinas, and Cerro Negro faults; *Costa et al.*, 2006) are primarily associated with compressive deformation. Late Pleistocene lava flow and alluvial fan along the San Rafael Block show evidence of active faulting and folding (*Folguera et al.*, 2009; *Branellec et al.*, 2016a).

3 Methods and Data

3.1 Structural Seismic Interpretation

The interpretation of an unpublished Post-Stack Depth Migration (PSDM) seismic line (5185-ATUEL-NORTE-SCAN2004; courtesy of TOTAL SA) complemented by stratigraphic constraints from the well YPF.MdN.S.a-15 (Figure 4), enabled us to reconstruct the unexposed Sosneado fault ramp at depth and estimate its Quaternary slip rates. Although we are not authorized to formally publish the seismic line, we share here our interpretation of the seismic reflectors (Figure 4). Our interpretation is based on a depth-converted 2D seismic line available to us. We did not have access to the velocities or other parameters used in the depth conversion process.

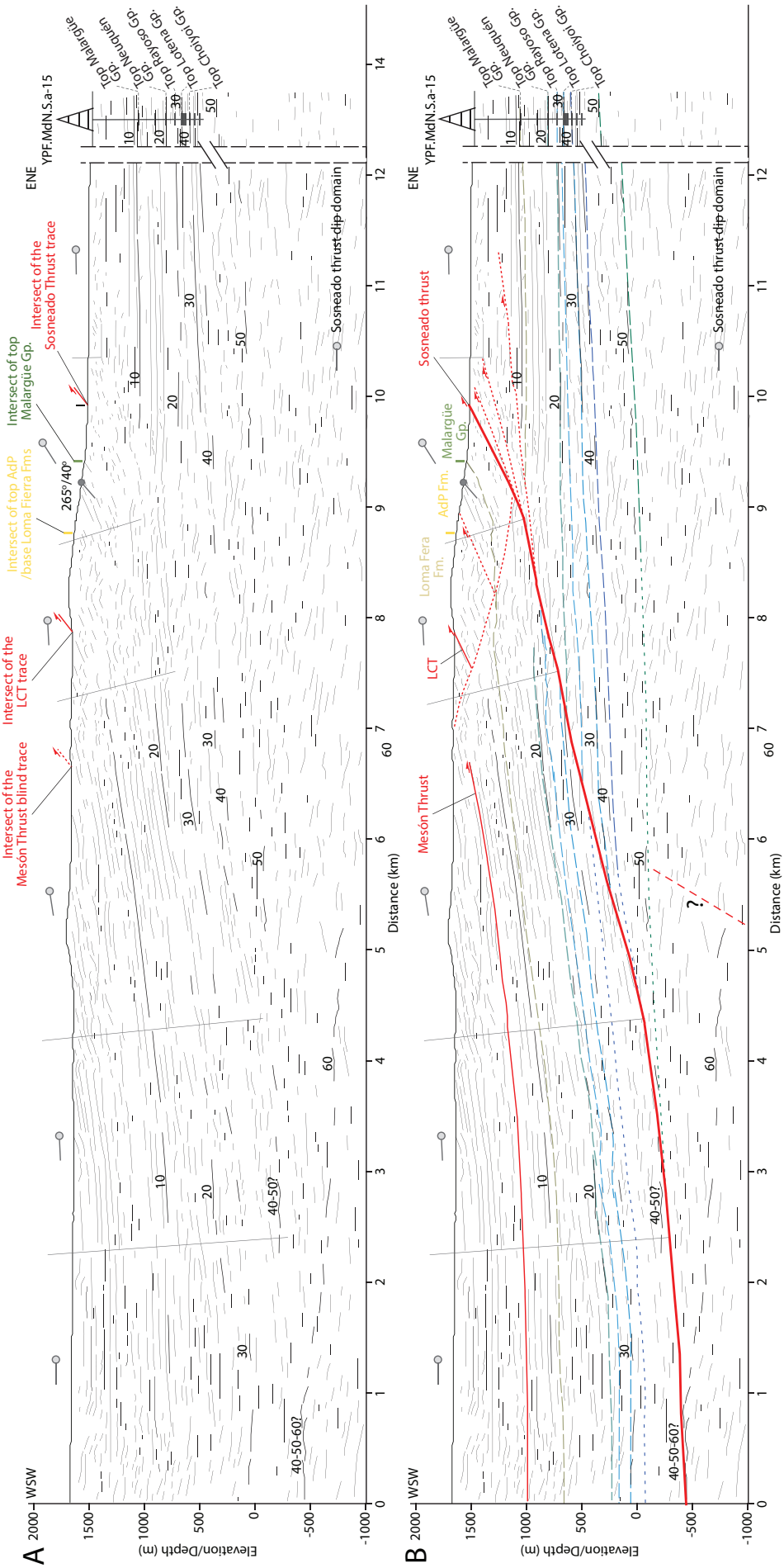

Figure 4 – Skeleton interpretation of the seismic line 5185-ATUEL-NORTE-SCAN2004 (PSDM). Dip domains are represented above the topography, and labels 10 to 60 refer to key seismic reflectors with a continuum mappable all along the line.

Our structural and stratigraphic interpretations of the hanging wall of the Sosneado Thrust were deduced from our updated structural map of the area (Figure 2). Faults mapped as dashed lines in Figure 4B were interpreted solely from the seismic section, with no confirmation at outcrop. In order to tie the stratigraphy of outcrops with the well, we have numbered key seismic reflectors, labelled by numbers reflecting their respective stratigraphic order of deposition (low numbers older, high numbers younger) (Figure 4B). The mapped reflectors have distinct seismic characters, and can be mapped throughout the line without the well data (Figure 4A). The intersection of reflectors mapped across the line within the well confines our interpretation of stratigraphic units. The dips of the reflectors were grouped in dip domain boundaries or discontinuities (i.e. faults) (Figure 4). To ensure that our seismic interpretation is balanced, we kinematically tested it and restored it back, honoring line length balancing, area conservation, and top/bottom continuity of layers in both the hanging wall and the footwall of the fault.

The shallowest segment of the ramp displays evidences of fault splays and duplexes forming second and third-order faults cutting the Neogene units in both the hanging wall and the footwall of the ramp (Figure 4B). We complemented our seismic interpretation with detailed observations and dip measurements at surface outcropping along and around the line. We have only estimated slip rates of the deeper segments of the main fault ramp, and not those of the secondary faults. To address slip rates of the latter, more extensive field mapping and control would be required. As for the main fault, the Sosneado Thrust is mappable precisely at depth on the seismic and it is well exposed at outcrop where it accommodates most of its slip. Our interpretation also takes into account secondary folds affecting the Mesozoic and Tertiary units. Secondary folds and faults within the Tertiary formations have been incorporated into the structural section and eventually in our structural restoration. We also considered the deformation and displacements along the Mesón Thrust. While it is not possible to estimate the slip along the secondary faults on the field, the shortening deduced from the restoration of our 2D seismic structural interpretation, is likely to provide a reliable estimate. There is evidence at outcrop for surface ruptures of secondary faults in the Quaternary sediments, but they cannot be used to quantify the total displacement on the main fault ramp.

3.2 Morphotectonic Analysis

Depositional and deformation geometries and relative ages of Quaternary deposits have been studied from field observations and remote sensing analysis. The first step was to identify and map Quaternary deposits in the study area using multispectral optical satellite images, geological maps, and digital elevation models (DEMs) (Figure 5; *Zöllner and Amos*, 1973; *Ramos*, 1981; *Leanza and Hugo*, 2001; *Nullo et al.*, 2004; *Giambiagi et al.*, 2008). For this study, we have used ASTER (Advanced Spaceborne Thermal Emission and Reflection Radiometer; *Kahle et al.*, 1991) and Landsat 7 (*Markham et al.*, 1997) images with a resolution of 15 and 30 m, respectively. Lithological units were identified from spectral radiance and texture on red-green-blue (RGB) colour combination of optical images. We ground-truthed and validated our remote sensing interpretations with analysis of sedimentary and morphological characteristics of deposits in the field. To improve accuracy of mapping of these deposits, we have used a combination of DEMs: the Shuttle Radar Topographic Mission data (SRTM DEM at a spatial resolution of 90 m and a vertical precision of 10-16 m) and stereo pairs of ASTER images (ASTER GDEM2 from METI and NASA, with a spatial resolution of 30 m and a vertical precision of 2-3 m). Additionally, we generated the longitudinal profile of the Atuel River and projected alluvial terraces using ASTER GDEM2 to identify any anomalies in the theoretical concave profile of the river bed.

3.3 Terrestrial in Situ Cosmogenic Nuclide (TCN) Dating

To constrain river incision, erosion rates and displacements, we dated depositional surfaces of exposed alluvial terraces using the TCN dating method measuring ^{26}Al and ^{10}Be isotopes. This method provides estimates of the residence time of clastic materials at the surface and dating of the ages of exposure (e.g., *Brown et al.*, 1991; *Brook et al.*, 1995; *Bierman et al.*, 1995; *Ritz et al.*, 1995; *Leland et al.*, 1998; *Siame et al.*, 2000). The limits of the technique are from the half-lives of ^{10}Be (1.36 $\pm$ 0.01 Ma) and ^{26}Al (0.72 $\pm$ 0.01 Ma), as well as the ages of erosion of the surfaces of the alluvial cones which do not exceed a few hundred thousand years.

The method assumes that, in orogenic systems, surface processes such as erosion, river transport and deposition of eroded materials happen in a short time lapse compared to the age of the depositional surfaces. During this process, the production of TCN is considered as negligible. The duration of subaerial exposition of clastic materials refer to the time when the depositional surface was inactive or abandoned. In dynamic landforms, the clastic deposits have already undergone TCN production during exhumation and transport process: this previously acquired TCN content is called inheritance (*Bierman*, 1994; *Hallet and Putkonen*, 1994; *Brown et al.*, 1995). The variable inheritance during the path to the final deposition is a limitation to the method, which then gives a maximum age of the depositional surfaces. In addition, after final deposition, clastic materials may have been first buried then exhumed, or hidden by any other materials or relief: this will lead to underestimate ages. To minimise the risk of

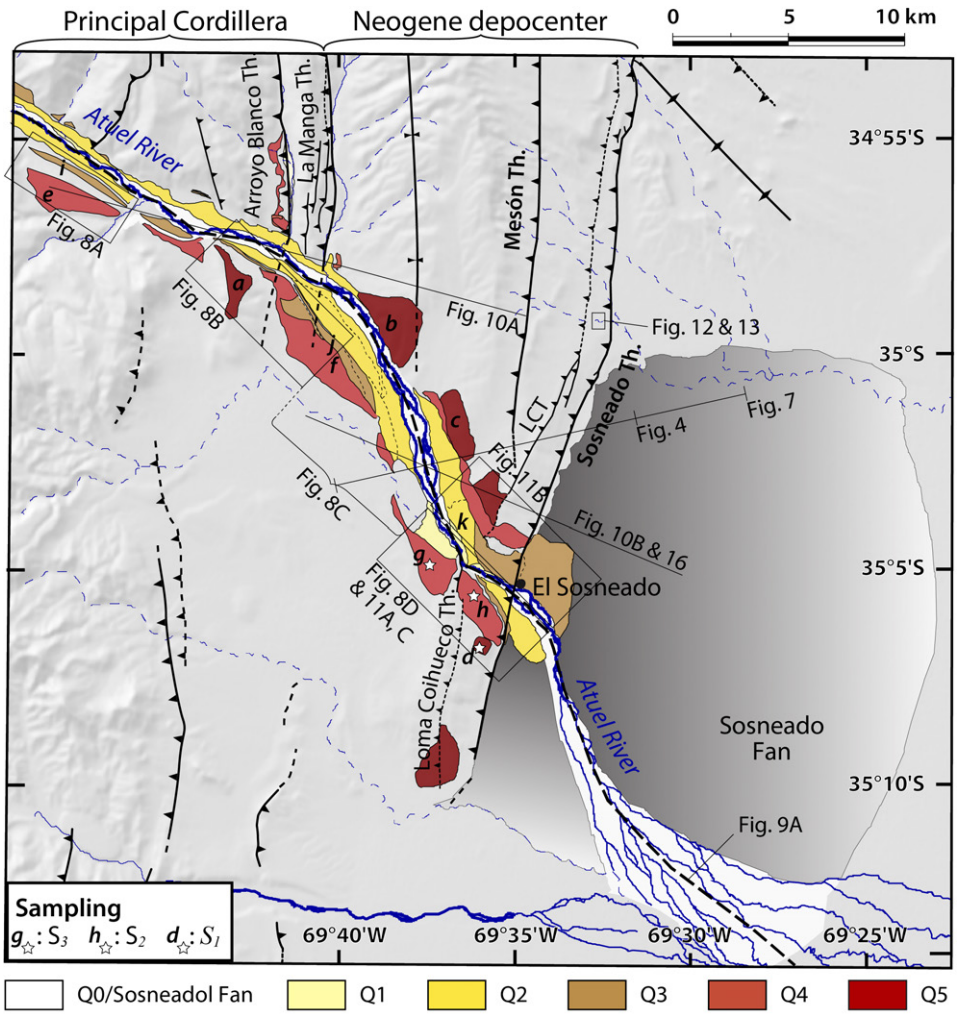

Figure 5 – Map of the Quaternary deposits, from ASTER and Landsat 7 images and on the field. Letters *a* to *k* are landmarks of the alluvial remnants projected orthogonally to the Atuel River longitudinal profile (Figure 9A).

sampling material with an age underestimation bias, for every surface studied several samples must be dated (*Cerling and Craig*, 1994; *Anderson et al.*, 1996). Our experience indicates that inheritance is either negligible or large enough to be detected (e.g., *Regard et al.*, 2005). Some authors partly overcome these issues through depth-profiles, a technique too costly to be implemented in this area.

In this study, we sampled alluvial quartz pebbles (sandstone, granite…) from alluvial terraces, avoiding areas with relief (scarps) or potentially eroded. By comparison with other locations in the world (*Portenga and Bierman*, 2011), in similar settings (e.g., *Baker et al.*, 2009; *Pepin et al.*, 2013; *Branellec et al.*, 2016a), the local erosion rate is expected to be less than 10 m/Ma. We chose samples likely to have rested in their original depositional configurations, i.e. partly enshrined in the ground (Figure 6). We used the couple $^{26}Al/^{10}Be$ to constrain inheritance uncertainties. ^{26}Al and ^{10}Be give similar ages for short periods of time typically less than a couple of hundreds of kyrs. Because the half-life of the ^{26}Al is shorter than the ^{10}Be, the concentration of ^{26}Al must be equal or lower than the latest ^{10}Be x R (where R ≈ 6.5 is the production ratio between ^{26}Al and ^{10}Be). If the ages given by ^{26}Al and ^{10}Be are the same, then the age estimate is robust. An ^{26}Al age older than a ^{10}Be age is quite impossible, and indicates technical issues during the laboratory processes. In this case, we consider the ^{10}Be result as the best approximation for maximum ages because it is technically more robust (D. Bourlès, pers. Comm.). If the ^{26}Al age is younger than ^{10}Be age, the pebble suffered at least one burial episode during its transport within the geomorphic system (*Granger and Muzikar*, 2001). In the following, we indicate the range of acceptable maximum ages in case of a possible burial stage. These ages are maximum ages because it is always possible to imagine the entire sample content has been acquired before its deposition on an alluvial terrace.

Samples were prepared and measured by the Accelerator Mass Spectrometry (AMS) at the National Laboratory for Cosmogenic Nuclides (LN2C, hosted by CEREGE, Aix-Marseille University) - see in Table S1 in the Supporting Information and Table S2 in Appendix for the resulting concentrations and measurements dataset. All ^{10}Be concentrations are normalized to $^{10}Be/^{9}Be$ SRM 4325 NIST reference material with an assigned value of $(2.79 \pm 0.03)\cdot10^{-11}$.

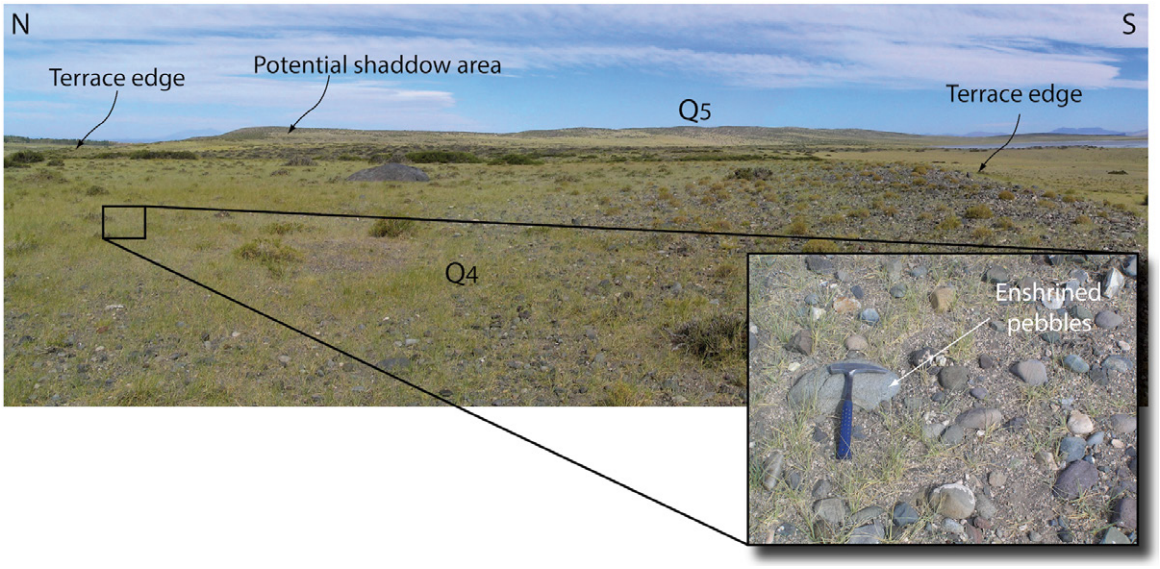

Figure 6 – Field picture of the sample site S5 (Q4) showing a sampled sandstone pebble, big and enshrined enough to decrease the risk of post-deposition displacement and located in the middle of the alluvial terraces to avoid shadow and erosional areas at the surface's edges.

This standardization is equivalent to 07KNSTD within rounding error. Analytical uncertainties (reported as 1σ) include a conservative 0.5% external uncertainty based on long-term measurements of standards, a one-sigma statistical error on counted ^{10}Be and ^{26}Al events, and the uncertainty associated with the chemical and analytical blank correction. The ^{10}Be/^{9}Be and ^{26}Al/^{27}Al blank ratios were (4.20 $\pm$ 1.63)·10^{-15} and (7.87 $\pm$ 5.57)·10^{-16}, respectively (see Table S1 in the Supporting Information).

4 Structural Configuration of the Sosneado Thrust at Depth

The Sosneado Thrust is described as a fault-bend-fold structure (*Giambiagi et al.*, 2008) located at the thin-skinned front of the Principal Cordillera. It cuts across Mesozoic sediments and Cenozoic syn-orogenic deposits. Sediments from the Malargüe Group (upper Cretaceous to Paleocene) are sparsely exposed at the bottom of the thrust scarp (Figures 2 and 7) while the Agua de la Piedra Fm. (middle Miocene) forms most of the outcrops along the frontal ridge (Figures 2, 3 and 7). There is some discussion regarding the dip of the thrust ramp, with estimates ranging from 50 to 60° (*López Ordines et al.*, 2022), 20 to 50° (*Fuentes et al.*, 2016), or 20 to 25° *Giambiagi et al.* (2008). The thrust is interpreted as detached either in the Upper Cretaceous (Figure 2B *Giambiagi et al.*, 2008) or in the Upper Jurassic-Lower Cretaceous (Tordillo and Vaca Muerta Fms; *Bechis et al.*, 2010; *López Ordines et al.*, 2022). *Fuentes et al.* (2016) suggest that the thrust detaches in the Lower Cretaceous north of latitude 35°S and in the Upper Cretaceous south of it.

Our seismic interpretation of the Sosneado Thrust indicates dips ranging from 12 to 26° whilst all stratigraphic units in the hanging wall are tilted to the west over a width of 7 kilometres (Figures 4 and 7). We note abrupt dip changes of the seismic reflectors labelled 20-50 across the ramp of the thrust fault all the way down to a depth of 500 meters below sea level (Figure 4; reflectors labelled 40-50). The ramp coincides with the trace of the Sosneado Thrust at the surface along with sediments of the Agua de la Piedra Formation (Middle Miocene) and the Malargüe Group (Upper Cretaceous-Paleocene) in the exposed hanging wall (Figure 7). The blind thrust with a low angle ramp between 1000 and 1500 m corresponds to the southern tip of the Mesón Thrust. The precise stratigraphic level of detachment in the fault hanging wall remains however unconstrained, as we do not have access to sufficient well data. However, we propose two hypotheses: a first one where the detachment of the thrust occurs in the upper Jurassic mudstones and evaporites of the Vaca Muerta/Tordillo Formations. This would require a thickening to the west of layers in between reflectors labelled 50-20 (blue unit in Figures 4 and 7) from 160 meters thick in the footwall to 470 meters thick in the hanging wall. A second one where the detachment level lies at the base of the igneous rocks of the Choiyoi Group, right above the Proterozoic-Permian crystalline basement (Figure 7). This has not been considered in previous studies (*Giambiagi et al.*, 2008; *López Ordines et al.*, 2022). The eastward tilt of the seismic reflector 60 meters below the Sosneado Thrust may relate to a west-dipping normal fault of the Mesozoic Atuel depocenter or may be due to the presence of thicker Upper Jurassic weak layers or the Middle Jurassic evaporites (Auquilco Formation) that localized the ramp initiation.

The presence of fault splays and duplex structures on both the hanging wall and footwall of the thrust ramp, indicated by variable seismic reflector dips (Figure 3A), is in agreement with observations

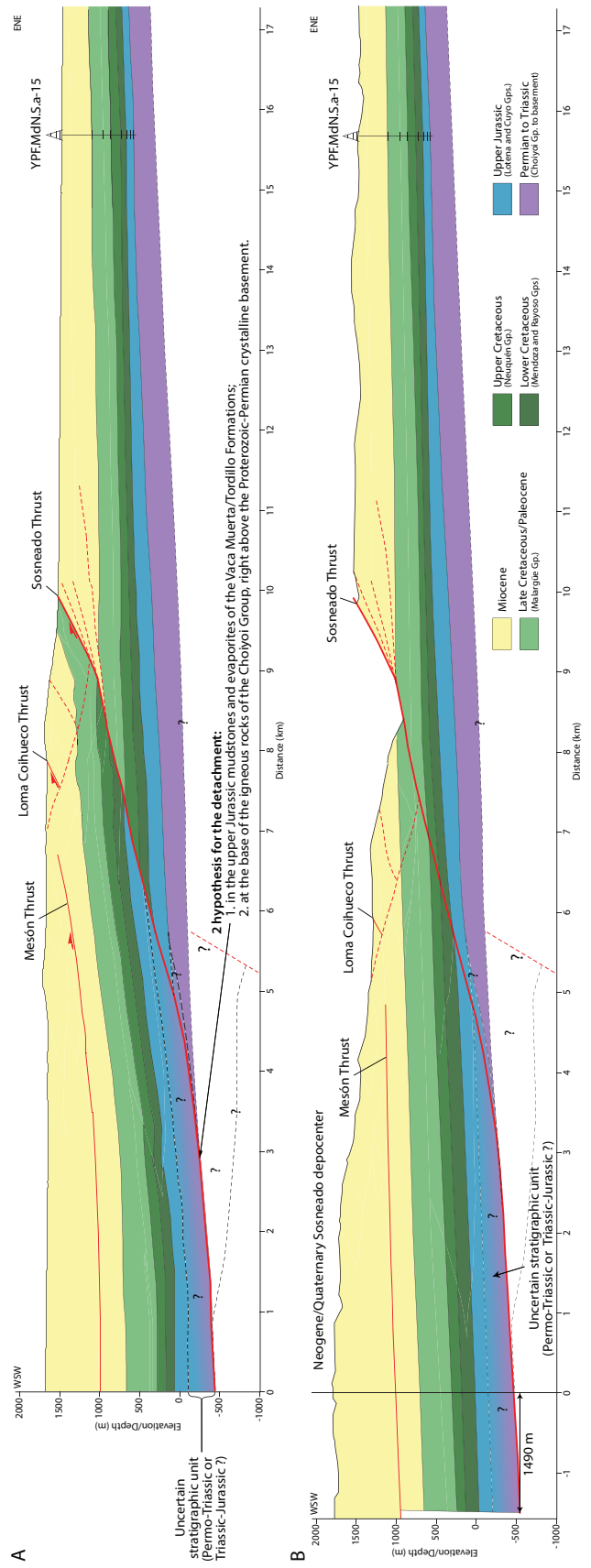

Figure 7 – **A-** WSW-ENE structural section of the Sosneado Thrust interpreted from the seismic line 5185-ATUEL-NORTE-SCAN2004 (PSDM, see Figure 3) and the well YPF.MdN.S.a-15 (location in Figure 2).; **B-** Restored cross-section giving a total shortening estimation of 1490 m on the Sosneado Thrust.

from field work and satellite imagery. Notably, our investigation reveals the presence of the Loma Coihueco Thrust (LCT) (Figures 2A, 3B, 4 and 7), which is accountable for secondary folding and exhibits limited displacement within the Neogene units as elaborated in the subsequent sections.

Our structural reconstruction suggests that the Sosneado Thrust is a thin-skinned low-angle reverse fault ramping above a regional detachment level located at approximately 500 m below sea level (b.s.l.) (*Bechis et al.*, 2010; *Fuentes et al.*, 2016) in agreement with previous interpretations (*Giambiagi et al.*, 2008; *Bechis et al.*, 2010; *Fuentes et al.*, 2016). Not accounting for quantification of subseismic scale folding or creep deformation, our kinematic restoration suggests a post-Miocene shortening of at least 1500 m (Figure 7), in agreement with another estimate obtained from seismic interpretation by *López Ordines et al.* (2022).

5 The Atuel River and Its Deposits

To study the possible ongoing activity of the Sosneado Thrust, we have focused on the deposits of the Atuel River. The river has a linear or meandering shape in a narrow alluvial plain (<200 m wide) across the Principal Cordillera and the Loma Coihueco ridge (Q0, Figure 4). Downstream of the La Manga Thrust further east, the river becomes anastomosed and flows in a wider alluvial plain (~700 m). East of El Sosneado locality, the river spreads over an even larger area, where lies the active depot zone of the broad Sosneado alluvial fan in continuity of Q0 (Figure 5). The Sosneado alluvial fan is about 20 km long from east to west and 25 km large from north to south, at an elevation that decreases from 1570 m in the west to 1410 m in the east, and with an average slope of 1%. Smaller alluvial fans are mapped along the Principal Cordillera at the toe of the Mesón and the Sosneado Thrusts north of El Sosneado locality (Figure 5).

The Atuel River dissects five alluvial terraces upstream of the El Sosneado Thrust. They are named Q1 to Q5 (Figures 5 and 8), where Q1 is the lowerstand and youngest and Q5 the highest and oldest. The remnants of Q2-Q4 alluvial terraces stretch continuously from the Principal Cordillera to the Sosneado fan, across a zone approximately 5 km wide and following the course of the Atuel River. Q1 and Q2 are made of pebbles smaller than 10 cm in diameter with a clay matrix. Q1 brackets the river across the Loma Coihueco Ridge and in the Principal Cordillera (Figures 5 and 8D). Q2 is the widest alluvial terrace between the La Manga Thrust and the Loma Coihueco ridge and narrows east of it (Figure 5). Q3 has a similar composition as Q1 and Q2 and partially preserved along the southern bank of the river in the Principal Cordillera, above the La Manga Thrust and the Loma Coihueco ridge (Figure 5). Q4 remnants are found all along the river (Figures 4 and 8) and consist of coarser conglomerates with pebbles of 20 cm in diameter. From the Principal Cordillera to

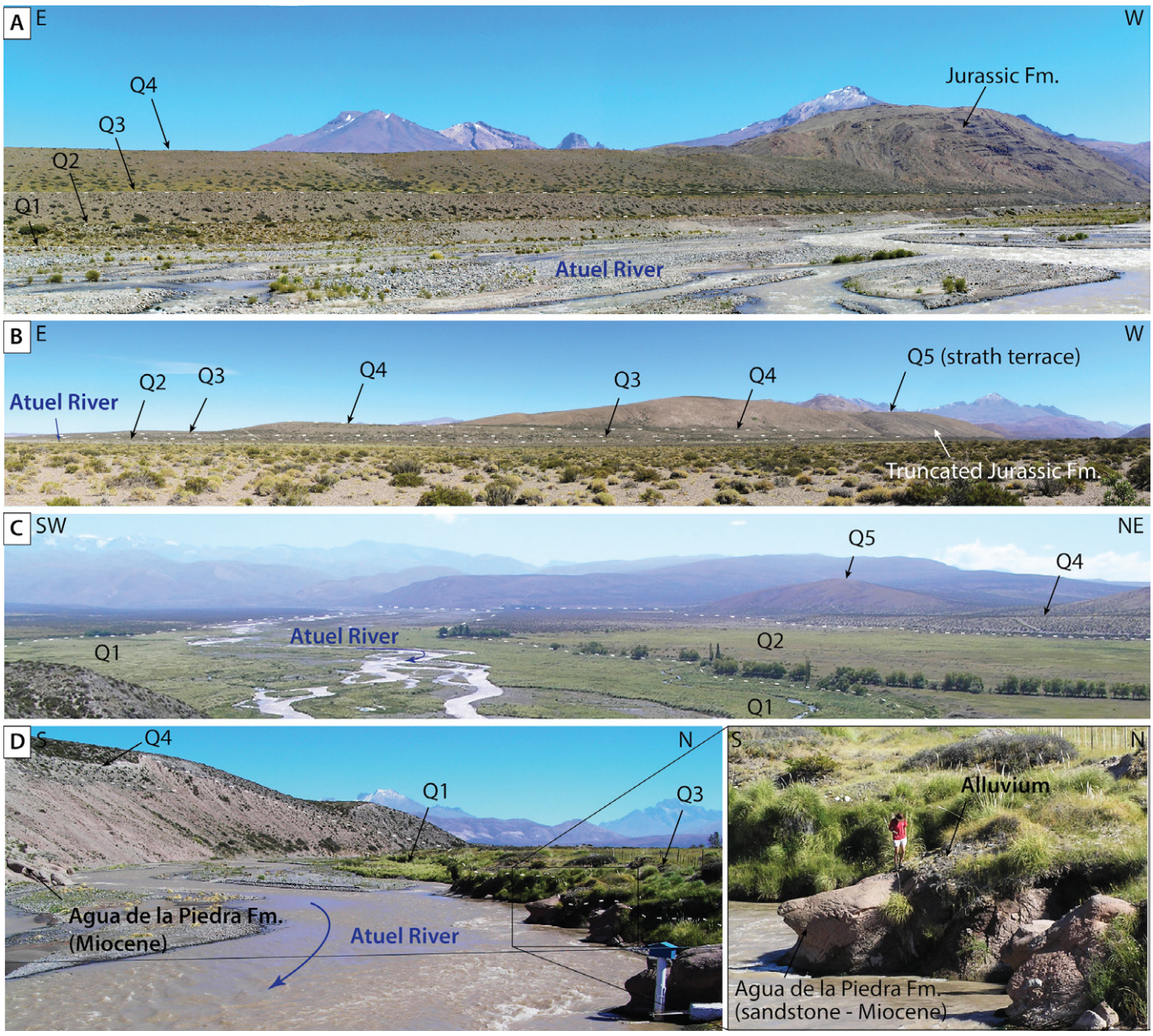

Figure 8 – Field photographs of quaternary terraces along the stream of the Atuel River (see locations on Figure 5): **A-** Fill-cut/Cut-and-fill Q2-Q4 terraces with the Eastern Principal Cordillera; **B-** Fill-cut/Cut and fill Q2-Q4 terraces at the southern tip of the Arroyo Blanco/La Manga thrusts, along the southern bank of the Atuel River. Q5 is a strath terrace further upstream; **C-** Q0-Q2 aggradation within a large valley between the La Manga Thrust and the Loma Coihueco Ridge; **D-** Q1to Q4 strath terraces above the Loma Coihueco Ridge.

the La Manga Thrust downstream, these intervals exhibit either cut-and-fill or fill-cut characteristics (Figures 8A-B). Aggradation dominates in between Q0 and Q3 downstream the La Manga Thrust where the valley widens (Figure 8C). Q2 appears to overlap Q3 with no evidence of cut-and-fill or fill-cut (Figures 8C). Intense lateral incision may have led to the erosion of Q4. Above the Sosneado Thrust, Q1 to Q4 are strath terraces (Figures 8D). Eventually, aggradation since at least Q3 shapes the Sosneado Fan downstream the Sosneado Thrust.

Remnants of Q5 are sparsely exposed along the Atuel River and southward of the Salado River. They reach a thickness of 30 m with pebbles from 1 to 30 cm in diameter above the Loma Coihueco Ridge (Figures 5 and 8C). An erosional surface topographically consistent with the top of Q5 (a in Figure 5) downstream, truncates the Jurassic formations above the Arroyo Blanco thick-skinned thrust that forms the tectonic front of the Malargüe FTB (Figures 5 and 8B). The La Invernada and Mesones formations are the oldest alluvial fans related to the Diamante River, and span over 30 km east of the catchment outlet of the Principal Cordillera (*Giambiagi et al.*, 2008; *Baker et al.*, 2009). They truncate the Neogene synorogenic deposits north of the Atuel River (Figure 2). The nature of the Q5 remnants is ambiguous. On the northern bank of the Atuel River, along the Cuchilla de la Tristeza syncline (Figure 2, and labelled b in Figure 5), they may be fill-cut or cut-and-fill alluvial terrace within the Mid-Pleistocene alluvial fans of the La Invernada and Mesones Fms. Q5 is rather a strath terrace upstream

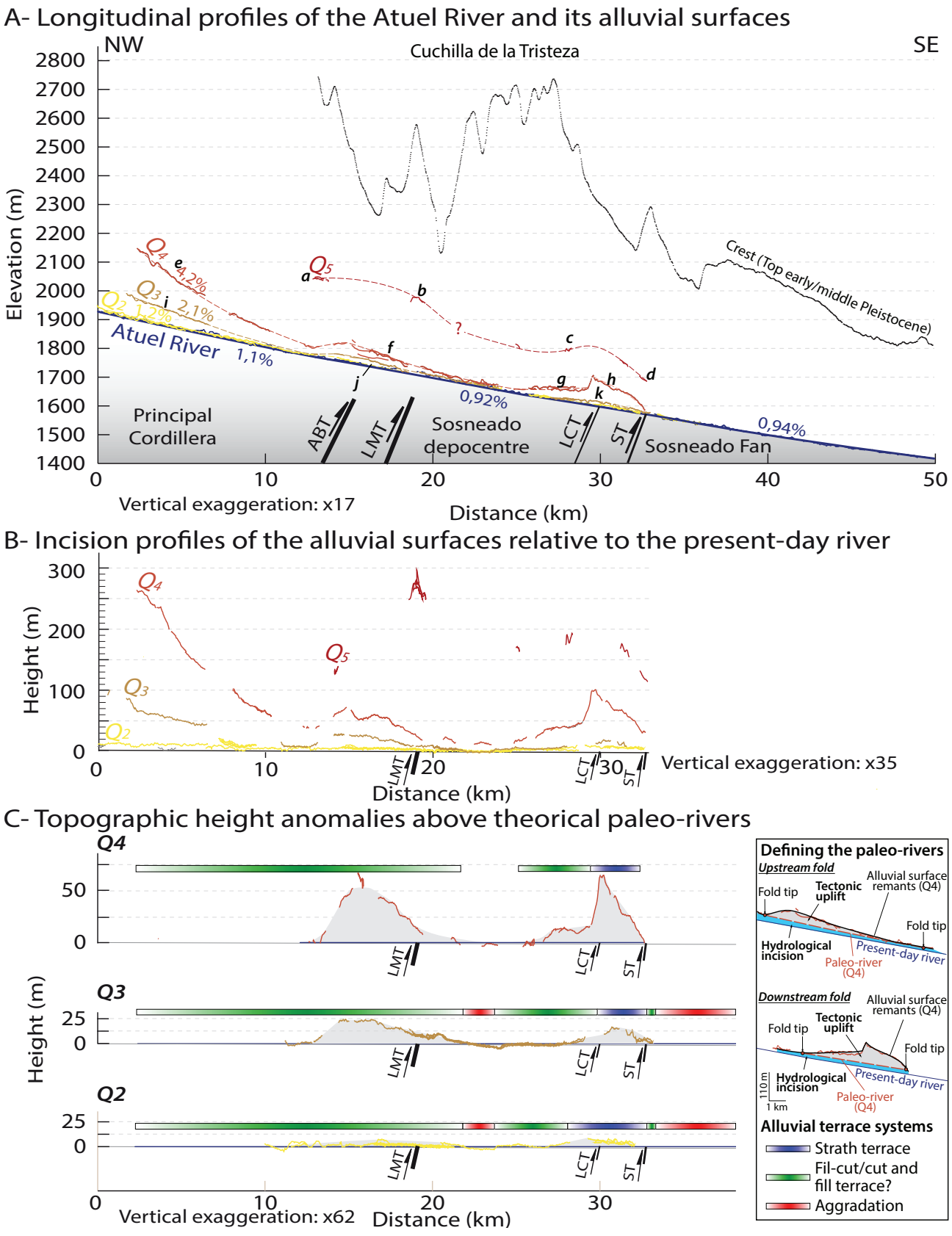

Figure 9 – Longitudinal profile of the Atuel River (blue line) and its alluvial terraces (yellow to red color scale) from the Principal Cordillera to the Sosneado fan. **A-** Remnants of the alluvial terraces projected perpendicularly to the river longitudinal profile. Elevations are from the ASTER GDEM (spatial and elevation resolutions of 30 m and 7-14 m, respectively). Interpolated dashed lines defining the longitudinal profile of each alluvial terrace interval. Black dots refer to the crestal topography along the river. Letters *a* to *k* are landmarks of the alluvial remnants on the Quaternary geological map (Figure 4). **B-** Longitudinal incision profiles of the tops of the alluvial terraces relative to the current bed of the Atuel River. **C-** Profiles of topographic anomalies on each terrace level relative to their ante-deformation river bed. The colored bars indicate the type of alluvial systems for the Q2-Q4 interval. LMT: La Manga Thrust; LCT: Loma Coihueco Thrust; ST: Sosneado Thrust.

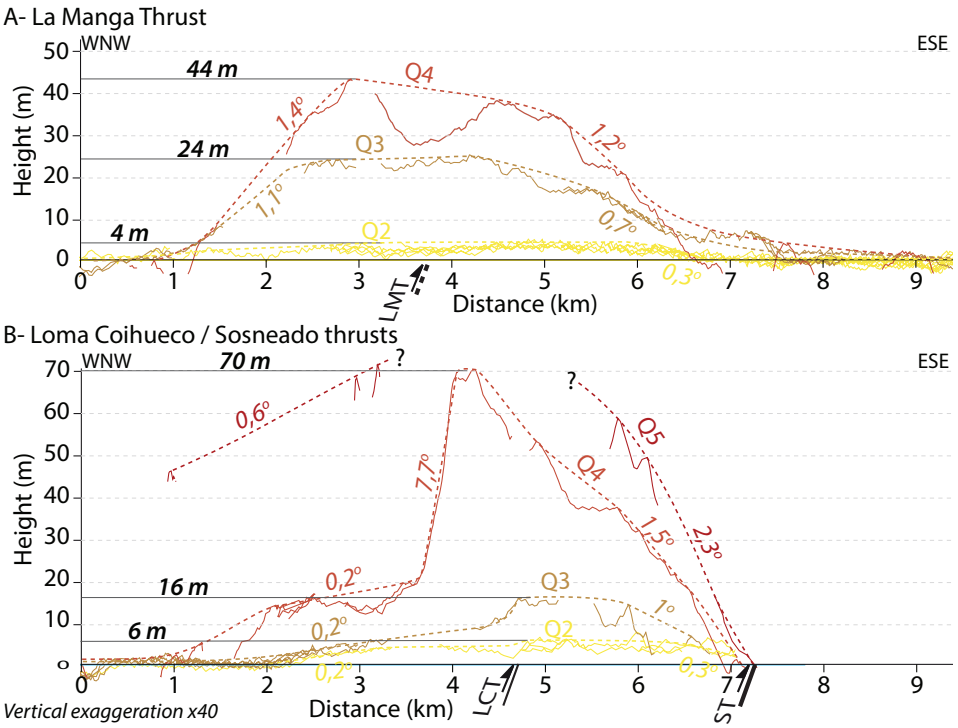

Figure 10 – Zoom-in of local progressive folding recorded by the profile of residual topographic height of the Atuel River terraces (Figure 9C), relatively to their respective paleo-river bed, and projected perpendicularly to the Sosneado Thrust trace. **A-** A ~7 km-wide west-verging folding immediately south of the thick-skinned La Manga Thrust (LMT). **B-** A 5-6 km-wide east-verging folding above the Sosneado Thrust (ST). The Loma Coihueco Thrust (LCT) is responsible for the steep west-dipping segment of Q4 at the folding hinge (location in Figure 4). The solid lines represent the topographic data derived from the DEM, while the dashed lines depict theoretical terrace profiles, mitigating erosional effects.

the Arroyo Blanco and La Manga thrusts (labelled a in Figure 5 and Figure 8B) and above the Loma Coihueco Ridge (labelled c and d in Figure 5).

Figure 9A displays the topographic profile of alluvial terraces along the Atuel River, across the Principal Cordillera and the Sosneado fan. Figure 9B shows the longitudinal profiles of incision as recorded by the top of each alluvial unit, interpreted as abandoned and uplifted paleo-river beds. At Present, he Atuel River displays a concave-up shape with a total elevation difference of 420 m over 45 km (Figure 9A). The regional slope gradually decreases across the Western Principal Cordillera (1.1%), the foothills (0.92%) and gently increases above the frontal ridge (0.94%). The numerous and dense occurrences of remnants of the terraces Q1-Q4 enabled us to confidently map and correlate them. The remnants mapped above Q4 are identified as Q5, as they fit with the shapes along the longitudinal profiles of Q1-Q4.

In the Principal Cordillera, the alluvial terraces Q1-Q4 projected on the river profile, display a concave shape flattening through time (4.2% for Q4, 2.1% for Q3, 1.2% for Q2, and 1.1% for Q1; Figure 9A). In the Principal Cordillera, the incision is the largest upstream kilometres 12 on Figure 9B (up to 250 m for Q4 and 70 m for Q3). Downstream the La Manga thrust, Q4 stands only 20 meters above the river bed, 250 m lower than in the Principal Cordillera, while Q2 and Q3 are almost at the river bed level. No lower terraces are exposed across the Sosneado Fan (Figure 9A and B).

The incision profiles displayed with respect to the modern river bed as shown in Figure 9B, is a good proxy to identify and quantify tectonic uplifts (*Lavé and Avouac*, 2000). The topographic anomalies between the top of the abandoned alluvial terrace, and an approximate undeformed paleo-river bed, represented as a straight line connecting the tips of the antiforms (see embedded caption in Figure 9C). In the absence of records documenting the temporal gradient and sinuosity changes of the river, such as those utilized by (*Lavé and Avouac*, 2000), this approach enables removing the hydrological incision related to climate or autogenic processes. We therefore estimate the uplift's shape as recorded by the top of the alluvial units (*Messager et al.*, 2014) along the stream of the current Atuel River. These profiles show two distinct gentle antiforms, one at the tip of the Arroyo Blanco-La Manga thrusts, and another above the Sosneado Thrust. They document an increasing elevation of the antiforms with their relative age, that can be interpreted as gradual folding of the paleo-river beds. We intentionally withhold such an analysis in the Principal Cordillera (kilometres 0-12 on Figure 9C) because we cannot constrain the paleo-river beds without discussing the residual steepness gradient of the incision (Figure 9A and B). This would require consideration for broad thick-skinned tectonic uplifts, as well as climatic and autogenic surface processes (*Gosse*, 1994), which is beyond the scope of this study.

The surveyed terraces observed on the field illustrate the interplay between tectonic uplifts and morphogenesis of the river and its deposits (Figures 8 and 9C). The folding of strath terraces above the Sosneado Thrust and the narrowing of the present-day riverbed suggest an increased potential for sediment transport and incision rates, most likely driven by tectonic uplift. Conversely, the aggradation observed upstream, associated with the braided river channel within a large valley, may indicate a diminished sediment transport due to the formation of tectonic barriers. The aggradation in the Sosneado Fan could be the river's sedimentary response as it attempts to equilibrate with a relatively lower base level in the context of upstream tectonic uplift.

6 Neotectonic Deformation at the Front of the Malargüe FTB

6.1 Morphological Record of Recent Tectonic Activity: the Atuel River's Terraces

Figure 10 is a close-up view of the profiles of residual topographic anomalies that formed the two antiforms on Figure 9C, projected perpendicular to the fault traces. This allows quantifying more precisely the width and vertical uplift related to the slip on the thrusts' ramp. Terraces Q2 to Q4, positioned above the Arroyo Blanco and La Manga thrusts (ABT and LMT), form a broad 7 km-wide antiform, with vertical amplitudes increasing from 4 m for Q2, 24 m for Q3 to 44 m for Q4 (Figure 10A). The antiform is slightly asymmetric with a steeper western flank and more shallowly dipping eastern flank. Surfaces dip from 1.1° within Q3 to 1.4° within Q4 in the western flank, and dip from 0.3° within Q2, 0.7° within Q3 to 1.2° within Q4 in the eastern flanks.

Downstream, the Sosneado Thrust (ST) bounds the other antiform to the east. This antiform is 6 km wide within the Q4-Q5 interval and 5 km wide for the Q2-Q3 interval (Figure 10B). The amplitude of the bulge relative to the paleo-river bed increases from 6 m for Q2, 16 m for Q3, to 70 m for Q4. The eastern flank is the most steeply dipping, with slopes ranging from 0.3° for Q2, 1° for Q3, 1.5° for Q4, and 2.3° for Q5, while the western flank dips westward from 0.2° for the Q2-Q4 intervals, to 0.6° for Q5. The profiles of the residual topographic anomalies of the interval Q2-Q5 are disrupted above the Loma Coihueco Thrust (LCT), where the surface's slope reaches up to 7.7° dip in Q4 (Figure 10B). In both domains, the sparsity of remnants of Q5 hinders the estimation of the amplitude of the antiform.

We interpret these antiforms as the result of local uplifts associated with Quaternary deformation around the southern nose of the Arroyo Blanco-La Manga thrust system, and concomitant activity on the Sosneado Thrust. This interpretation is substantiated by the fact that the wavelength of these folds ranges from 5 to 7 km and are comparable to the one interpreted from seismic on the hanging wall of the Sosneado Thrust (Figure 7). The correlation between the amplitude of the antiform and the age of terraces suggests that deformation was continuous throughout the Quaternary sedimentary record. The amplitude of the tectonic folding indicates a minimal uplift, considering that the top of the surface may have been buried by aggradation on both sides of the Sosneado Thrust (i.e. *Lavé and Avouac*, 2000). Additionally, there is evidence for deformation of lower wavelength in the hanging wall of the Sosneado Thrust linked to the Loma Coihueco Thrust. Both thrusts are therefore contemporaneous.

6.2 Folding and Faulting of the Atuel River Terraces Above the Sosneado Thrust

The Loma Cohueico Ridge spans over a length of 10 km and a width of 5 km, south of the Atuel River. It is capped by Q4 and Q5 strath terraces (Figures 3, 5 and 11A), at its highest elevation point. The top of Q4 reaches an elevation of 1700 m, 70 m above the river bed. Two kilometres downstream, Q4 stands at 1630 m high, only 40 m above the river. Upstream of the ridge, Q4 does not exceed 1650 m, indicating that the dip of Q4 is not uniform and even locally reverse to the current river slope (0.5°) (Figure 11A). Similarly, above the northern segment of the topographic ridge extending north of the Atuel River, upstream of the ridge, Q4 remnants are found at 1660 m high and downstream at 1620 m high (Figure 11B). It reaches 1695 m high at its outer hinge.

At the northern edge of the ridge, a natural section along the southern bank of the Atuel river reveals outcrops at the bottom of Q4. As part of the western flank of the ridge, Q4 is tilted at 40° to the west and parallel to the underlying red beds of the Agua de la Piedra Fm. (Miocene) (Figure 11C). Along the axis of the ridge, both the Miocene shales and the tilted Q4 override to the East sub-horizontal Q4 alluviums (Figures 3A and 11A-B). This results in a subsidiary N-S trending 50 m-height scarp disrupting the top of the Loma Cohueico Ridge over 5 km (Figures 2 and 3A). This thrust dips approx. 40°W in the folded hanging wall of the Sosneado Thrust, folding and offsetting Q4 (Figures 3A and 11A, C). This subsidiary deformation in the hanging wall of the Sosneado Thrust, located south of the Atuel River, provides evidence of its activity after the deposition of Q5 and Q4. These observations align with the deformation patterns associated with the Loma Coihueco Thrust, as evidenced in the longitudinal and incision profiles of the terraces along the Atuel River (Figures 9 and 10B).

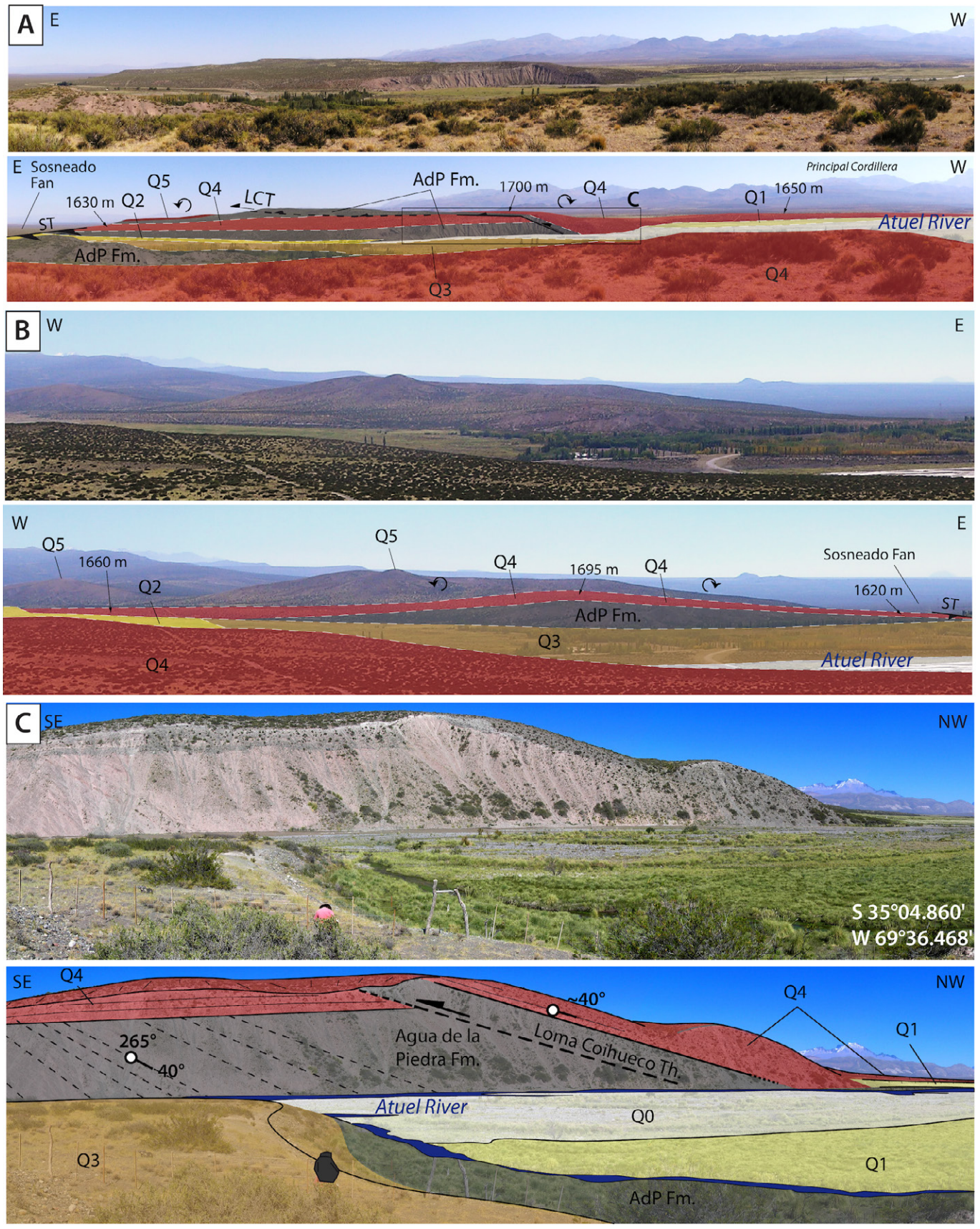

Figure 11 – **A-** The Loma Coihueco Ridge, south of the Atuel River, is the morphological expression of the hanging wall of the Sosneado Thrust (see locations on Figure 5). The ridge consists of outcrops of west-dipping Neogene deposits capped by a ~7 km-wide fold in the strath terraces Q4 and Q5 while the hinge of the ridge is affected by the subsidiary west-dipping Loma Coihueco Thrust (LCT). **B-** The strath terrace Q4 north of the Atuel River is folded above the Loma Coihueco Ridge. **C-** Zoom-in on the Loma Coihueco Thrust (LCT) back-tilting Q4 in the Sosneado Thrust (ST) hanging wall, along the southern bank of the Atuel River (location in A).

Table 1 – Dating Results: description and location of samples S2 (Q5), S4 and S5 (Q4). The dating is based on Terrestrial in situ Cosmogenic Nuclide (TCN) ^{10}Be and ^{26}Al via the Web Cronus Calculator (*Balco et al.*, 2008). The calculations were performed at constant production rate (*Lal* (1991)/*Stone* (2000)) assuming an erosion rate of zero. The SMA standard used by the CEREGE is the 07KNSDT (for more details refer to website: https://hess.ess.washington.edu/math/docs/al_be_v22/al_be_docs.html). The half-lives are 1.36 Ma and 0.72 Ma for the ^{10}Be and ^{26}Al, respectively. See Figure 14 and Table S3 in the Supporting Information for the detailed analytical results.

Sample name (Site(i)-sample(j))	Alluvial level	Latitude (DD)	Longitude (DD)	Elevation (m)	[^{10}Be] (10^5 atoms.g^{-1})	[^{26}Al] (10^5 atoms.g^{-1})	R ([^{26}Al]/[^{10}Be])	Average ^{10}Be and ^{26}Al exposure ages
S2-s1		-35.11	-69.6	1700	10.49 ± 0.31	43.86 ± 4.39	4.18	
S2-s3	Q5	-35.11	-69.6	1700	10.89 ± 0.36	59.21 ± 5.92	5.44	74.73 ± 8.07
S2-s4		-35.11	-69.6	1700	9.95 ± 0.33	30.96 ± 3.10	3.11	
S4-s1		-35.09	-69.61	1700	13.17 ± 0.39	76.55 ± 7.66	5.81	
S4-s2		-35.09	-69.61	1700	17.28 ± 0.46	79.08 ± 7.91	4.58	
S4-s3	Q4	-35.09	-69.61	1700	89.36 ± 0.29	61.85 ± 6.18	6.92	70.51 ± 7.51
S4-s4		-35.09	-69.61	1700	10.08 ± 0.29	105.60 ± 10.58	10.49	
S4-s5		-35.09	-69.61	1700	10.77 ± 0.31	74.60 ± 7.46	6.93	
S5-s1		-35.07	-69.64	1660	13.08 ± 0.40	86.25 ± 8.63	6.6	
S5-s2	Q4	-35.07	-69.64	1660	10.08 ± 0.29	65.20 ± 6.52	6.47	70.82 ± 7.08
S5-s3		-35.07	-69.64	1660	9.28 ± 0.36	55.03 ± 5.50	5.93	
S5-s4		-35.07	-69.64	1660	14.64 ± 0.43	43.04 ± 4.30	2.94	

6.3 Folding and Faulting in Adjacent Quaternary Alluvial Deposits Above the Sosneado Thrust

To the north of the Atuel River, the hanging wall of the Sosneado Thrust is covered by subhorizontal, unconsolidated alluvial deposits that are not associated with the Atuel River. The deposits are dominated by channel bedforms (20-30 cm-thick) filled by angular pebbles up to 10 cm in diameter, and interbedded with shaly and sandy sequences. These alluvial deposits cap unconformably the westward-dipping beds of the Agua de la Piedra Fm. (middle Miocene) and Malargüe Gp. (upper Cretaceous-Paleocene) (Figures 2B and 5). The deposits are lower in elevation than the Mesones Fm. (middle Pleistocene *Polanski*, 1962), and are therefore younger. Twelve kilometres north of the Atuel River, narrow erosive gullies incise the ridge (Figures 12 and 13) and expose its stratigraphy. The uppermost unit consist of a whitish colluvium, about 1 meter thick, gently dipping eastward and thinning westward. It overlaps an alluvial fan sequence (Figure 12) with a conglomeratic bed dipping 30°to the east due to, at least in part, if not totally to younger tilt and folding. The fan-like shape of the colluvium suggests that folding was also still ongoing during its deposition.

Around 200 m upstream, a 20-30 m-long trench exposes reverse faults within the same alluvial unit (Figure 13A). At least two faults, labelled Fault A and Fault B, offset six units (labelled *a* to *f*) consisting of conglomeratic channels, shales, and sand beds along the southern riverbank. The opposite riverbank displays a similar sequence of faults, again two faults cutting here through only four units (labelled *a'* to *d'*) (Figure 13B). The fault planes are irregular but consistently dip westward, in between 25 and 30°. Along the southern bank, Fault A offsets conglomeratic units *a* and *c* (Figure 13A). In the riverbed, it forms a shear zone cored by intensely deformed shales. Fault A is sealed in unit *d* (shale), which is significantly thickest in the footwall of the fault. The upper part of unit *d* and the base of unit *e* (conglomeratic) are gently folded, implying that Fault A was still active during the deposition of unit *e*. The fault offset reaches 30 cm in unit *c*. Above Fault A, Fault B consists of a 30 cm-long segment that offsets the base of unit *e* by 10 cm (Figure 13A). Unit *e* at the tip of the fault, is folded in an anticline. The fault does not appear to affect the underlying units.

On the northern wall, Fault A' cuts through units *a'* and *c'* with a consistent offset of 20 cm (Figure 13B), and no evidence for thickness variation, while unit *d'* on top is undeformed. This suggests that the fault became inactive after the deposition of unit *c'*, and before deposition d'. Fault B' cuts through units *a'* to *c'* and terminates in unit *d'*, which is significantly folded at the fault tip (Figure 13B). The offset measured along Fault B' decreases upward from 100 cm in unit *a'* to 70 cm in unit *c'*. This suggests fault activity throughout the deposition of the alluvial fan.

The facies and thicknesses of corresponding units on both sides of the gully shows comparable characteristics (Figure 13). The conglomeratic channels labelled *a-a'* and *c-c'* have similar thicknesses on both walls of the trench of approx. 1 m and 30 cm, respectively. Unit *a'* exhibits a coarser texture in the footwall of Fault A' (Figure 13A), while unit *c'* appears as a more extensive channel in the northern wall (Figure 13B). Additionally, unit *e'* is absent in the northern bank, whereas d' is significantly thicker (Figure 13B) compared to unit

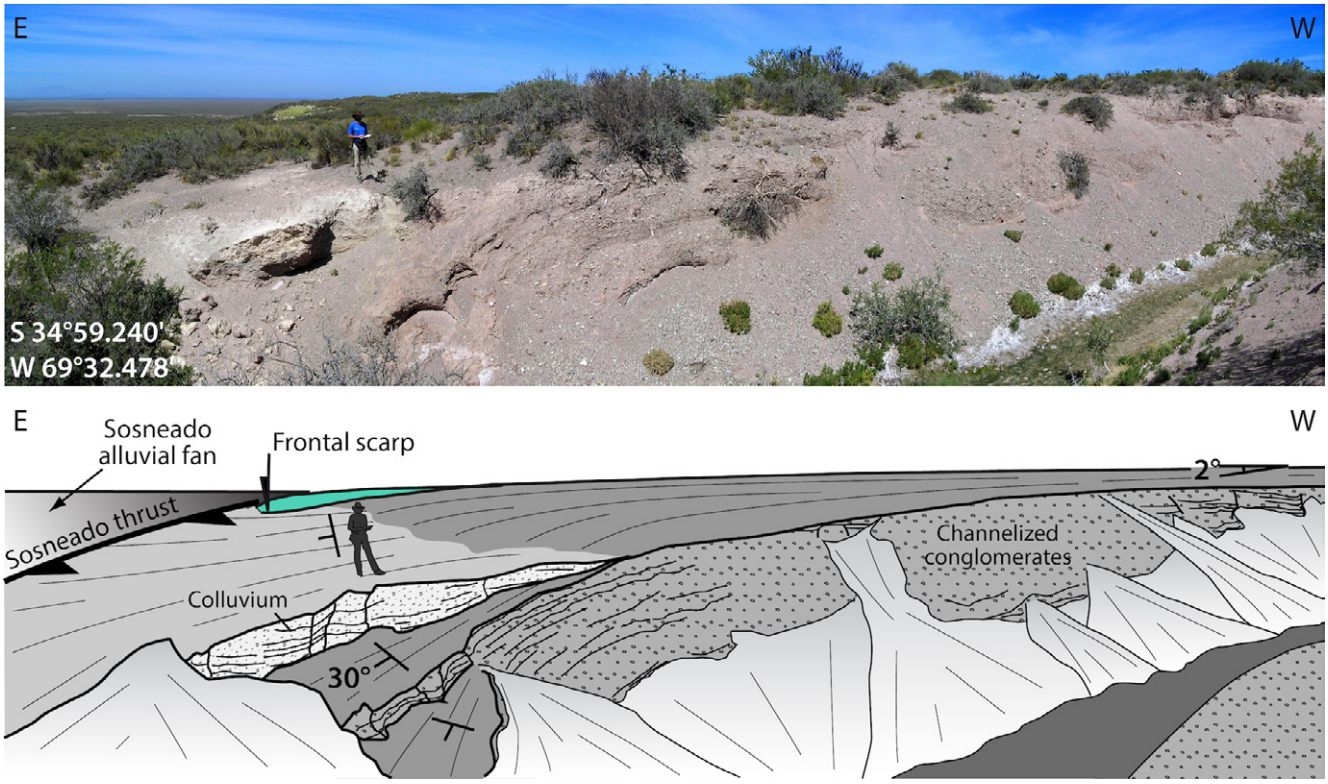

Figure 12 – Folding of alluvial fan deposits in the Sosneado Thrust hanging wall (location in Figures 2A and 5): channelized conglomerates are folded to the east and overlapped unconformably by synfolding colluvium.

d (Figure 13A). These variations are relatively minor considering the abrupt variability in extent, thickness, and pebble content often encountered in alluvial channels. Faults A and A' display similar geometries and offsets and disrupt the same units. We interpret them as two traces of the same fault, dipping WSW (N250°). Faults B and B' significantly offset the more recent units (*d*-*e* and *d*'). They are interpreted as two segments of the same fault, with segment B' representing the lateral termination of the main fault plane. These syn-sedimentary folding and thrusting structures within the alluvial fan provide additional evidence for activity of the Sosneado Thrust fault system during the late Quaternary.

7 Absolute Dating of Q4 and Q5

We sampled three sites along the right bank of the Atuel River to date Q5 and Q4. We selected three pebbles on Q5 surface above the Sosneado Thrust (Site 1, h in Figure 2), four pebbles of Q4 surface at Site 2 (l in Figure 2) and five pebbles of Q4 surface at Site 3 (k in Figure 2) upstream of the Loma Coihueco Thrust (Table 1). Each sample is referred to by its collection site number (S(i)) followed by a sampling index (s(j)). For example, pebble 3 in site 2 will be referred as S2-s3.

^{10}Be and ^{26}Al exposure ages are computed with both constant and non-constant production rates and show similar results even if the ^{26}Al exposure ages are slightly younger (4-5 kyr offset Table 1). We consider that results are robust when ^{10}Be and ^{26}Al ages are in close agreement (less than 5 kyr). Where they differ, we consider ^{10}Be ages as the most pertinent. In the following sections, we only consider the given ages with constant production rate.

The three samples from Site 1 (Q5) yield a quite robust ^{10}Be age of 75 $\pm$ 8 ka (Table 1 and dashed area in Figure 14). The younger ^{26}Al ages suggest a more complex history, possibly after deposition. Indeed, the ^{26}Al/^{10}Be ratios (3.11, 4.18 and 5.44, from Table 1) for these samples suggests a considerable transient burial during 1500 to 400 kyrs (S2-s4 and S2-s3, respectively), then a subsequent erosion upstream in the Andes. If the burial predates deposition these ages are overestimated, but if the burial took place after deposition, for example by a transient aeolian cover, then their ages are likely to be underestimated by this dating technique. However, given the similarity between ^{10}Be and ^{26}Al exposure ages, we propose that this effect is minimal. Therefore, the age of 75 $\pm$ 8 ka is likely to reliably date the Q5 surface.

Sites 2 and 3 (Q4) yield similar exposure ages, even if the individual data are somewhat scattered. In this case, we consider the youngest (with less inheritance) ^{10}Be exposure ages, i.e. those with similar ^{10}Be and ^{26}Al ages (samples S4-s3, S4-s5, S5-s2 and S5-s3 ; Table 1 and Figure 14). We also use S4-s4 ^{10}Be age as ^{10}Be and ^{26}Al give different ages, the older age provided by the latter being technically impossible as explained above. Dating of the two sites (Table 1 and dashed area in Figure 14), indicate that the most likely age of Q4 is 71 $\pm$ 7 ka (from samples S4-s3, S4-s4, S4-s5, S5-s2 and S5-s3).

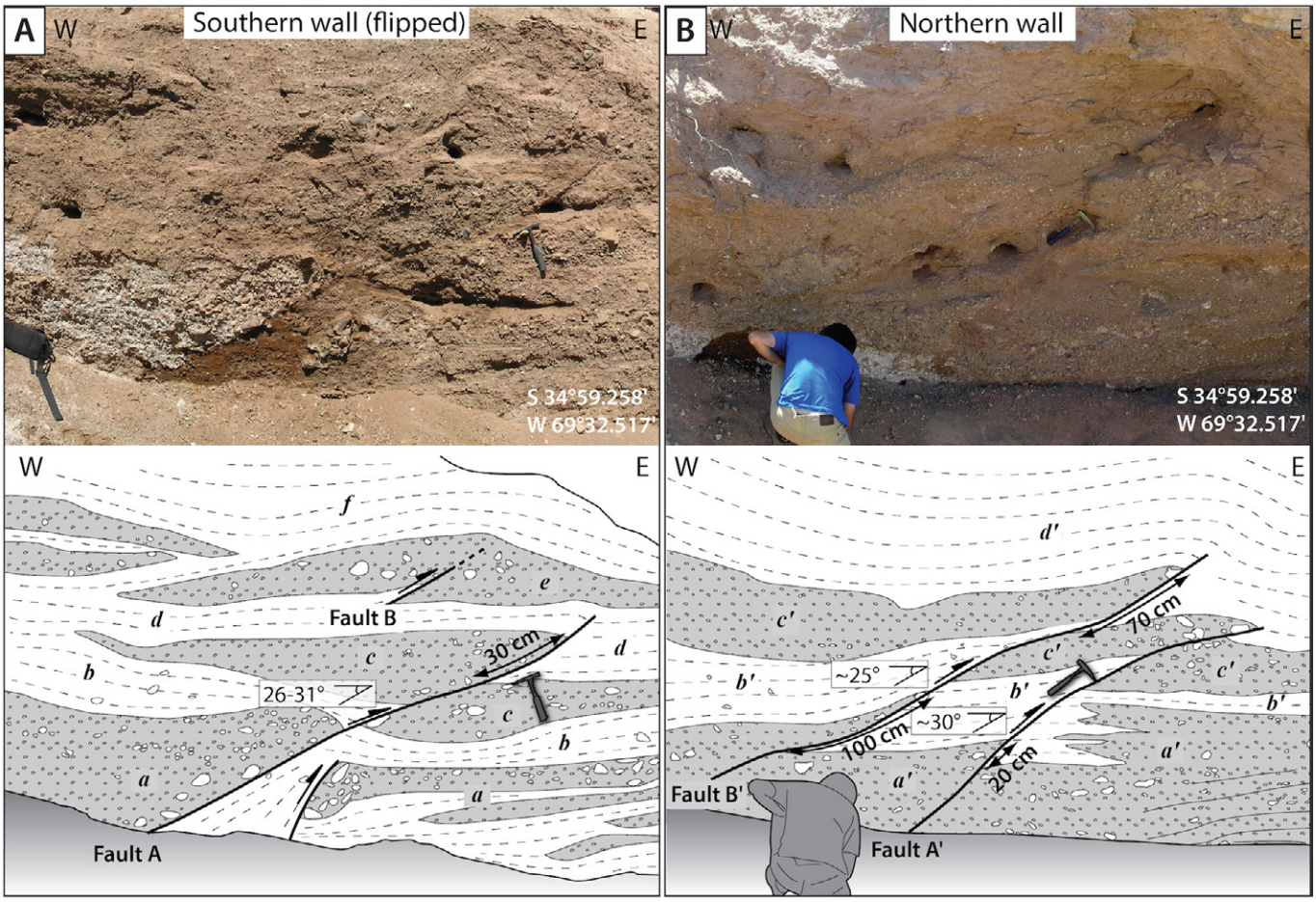

Figure 13 – East-verging reverse faults within alluvial fan deposits in the Sosneado Thrust hanging wall (location in Figures 2A and **5**) observed on both banks of a natural trench. Alluvial channels composed of conglomerates are labelled *a* to *f* and *a'* to *d'* along the southern and northern banks, respectively.

Cosmogenic dating yields exposure ages of 75 ± 8 ka for Q5 and 71±7 kyr for Q4 consistent with the geometrical arrangement of the alluvial remnants where Q4 is encased in Q5. Another point to keep in mind is that these values have been calculated with a null erosion rate. We discuss in the Supporting Information the impact of erosion rates on these cosmogenic ages.

8 Discussion

The gradual tilt and synsedimentary folding of the Mid-Pleistocene and Holocene alluvial systems (Q5-Q1) around the thin-skinned Sosneado Thrust and at the front of the thick-skinned Arroyo and La Manga thrusts result from the continuous uplift of the eastern border of the Malargüe FTB during the late Quaternary. This uplift impacted the morphogenesis of the Atuel River deposits leading to the genesis of strath terraces atop the Sosneado Thrust system, an anomaly by comparison with the other terraces elsewhere along the Atuel River (Figure 9). For example, there is evidence for local aggradation immediately upstream (Q3-Q0) and downstream (Q4-Q0) of the Sosneado Thrust. This pattern of incision and/or aggradation, alongside the location of thrusts, provide morphogenic markers of the ongoing uplift processes.

The Atuel River Valley provides exceptional exposures documenting Quaternary folding and faulting associated with Andean thin-skinned thrusts. Our aim was to date the alluvial terraces recording the deformation, quantify the deformation rates from with the folding and faulting of the terrace remnants and identify potential hazardous faults along the Principal Cordillera of the Malargüe region.

8.1 Alluvial Chronology and Regional Correlations

Cosmogenic isotope dating provides quite close absolute ages for Q5 and Q4 (75±8 ka and 71±7 ka, respectively), with incision between 80 and 200 m-deep of Q4 relative to Q5, as suggested by their incision longitudinal profiles (Figure 9B). Such time interval of 4±15 ka would imply a considerable incision rate of 20 to 50 mm.yr^{-1}, a high rate that is indicative of either sudden hydrological or climate factors, temporary high tectonic uplift, or possibly a dating errors.

Upon analyzing the cosmogenic data further, it was found that the ^{26}Al ages for Q5 were systematically younger than the ^{10}Be data (Table 1 and Figure 14). This difference may be due to the temporary storage

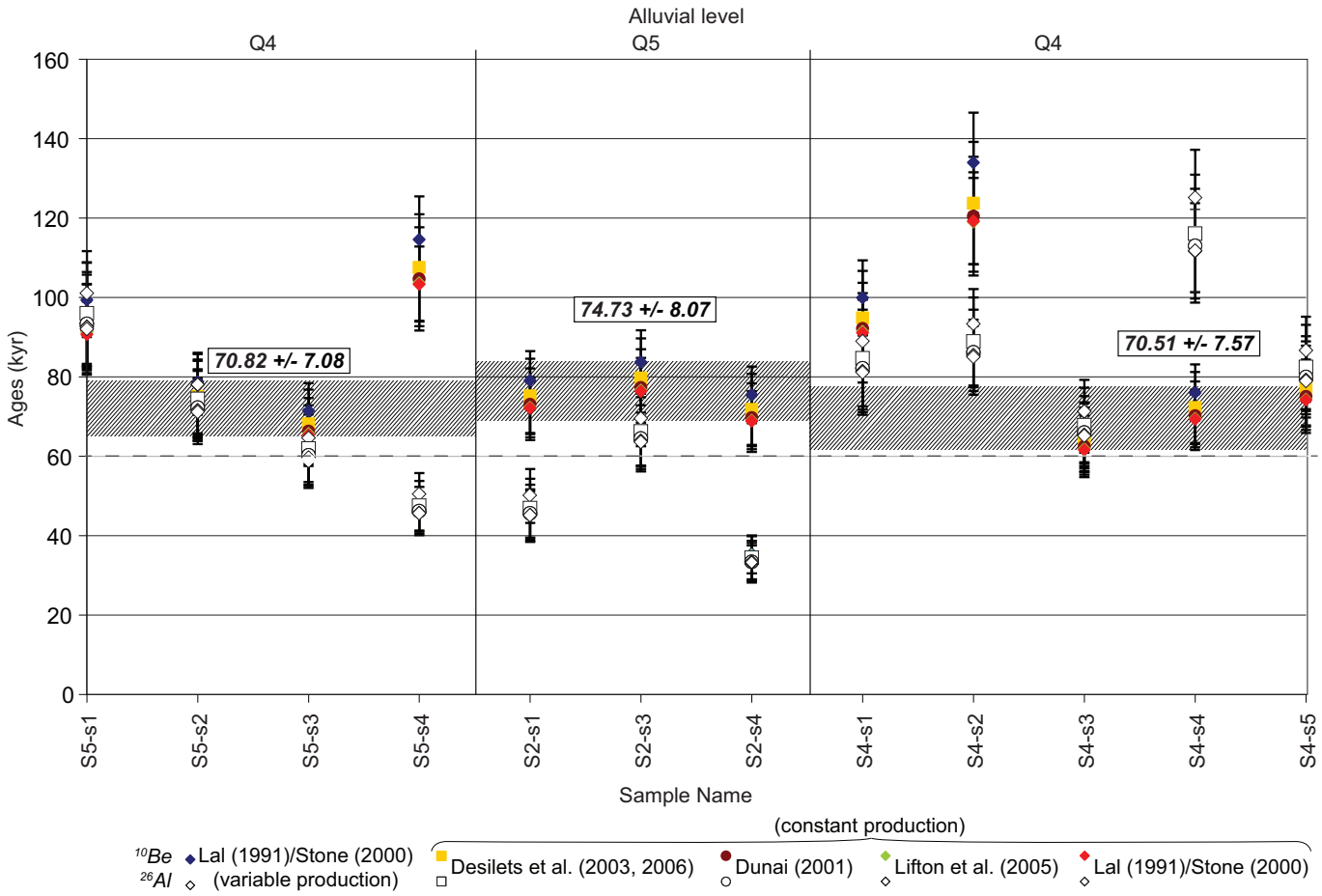

Figure 14 – Comparison of ^{26}Al and ^{10}Be ages calculated via the Web Cronus Calculator (*Balco et al.*, 2008) from (i) the method of *Lal* (1991)/*Stone* (2000) considering a constant production rate, and (ii) production rates varying according to the methods of *Desilets and Zreda* (2003), *Desilets et al.* (2006), *Dunai* (2001), *Lifton et al.* (2005) and *Lal* (1991)/*Stone* (2000).

of pebbles or a temporary coverage of the surface by eolian deposits. The latter explanation is consistent with other regional observations, which suggest the loss of an initial sedimentary cover over a period of a few hundred thousand years. Such scenario may explain the difference between the ^{10}Be and ^{26}Al data. However, the ^{10}Be and ^{26}Al datings for Q4 are consistent, two distant sites yielding similar results and implying that a temporary coverage over time is unlikely. Therefore, the age of 71 ± 7 kyr obtained for Q4 deemed reliable and likely.

In summary, our age estimates for Q5 and Q4 are 75 ± 8 kyr and 71 ± 7 kyr respectively. We cannot rule out the possibility of dating errors, but the end-members of the TCN dating uncertainties shows that their respective ages are in the range of 63-83 kyr with a maximum difference of age of 20 kyr.

The absolute ages for Q4 provide a chronological template of relative ages for other alluvial terraces thanks to regional correlations (Figure 15). Q5 likely postdates the middle Pleistocene Invernada and Mesones formations (Polanski, 1963). Considering the dating uncertainties, Q4 (71 ± 7 kyr) may be contemporaneous with surface Qt3 of the Diamante River (ca. 66-69 kyr; *Baker et al.*, 2009). *Gosse* (1994) estimated the age of the youngest terrace Q2 of the Atuel River to be of the last Marine Isotope Sequence, which correlates to the Qt5 remnants of the Diamante River dated to 13 ± 3 kyr (*Baker et al.*, 2009). Q1, only observed along the Atuel River, must be younger than Q2, i.e. 13 ± 3 kyr. Q3 would thus be temporally constrained between these two ages, corresponding to Qt4 of the Diamante River, which was dated at 22 ± 7 kyr (Figure 15 *Baker et al.*, 2009).

Considering the alluvial sequences of *Baker et al.* (2009), our age estimates for the alluvial terraces of the Atuel River are as follows: Q2 (13 ± 3 kyr), Q3 (22 ± 7 kyr), Q4 (71 ± 7 kyr) and Q5 (75 ± 8 kyr) (Figure 15). The last two age estimates being subject to caution as the incision rates in between the two units appear inexplicably anomalously high for the moment. The forthcoming analytical results on slipping rates may provide additional insights on to this issue.

8.2 Shortening and Slip-rate Estimations on the Sosneado Thrust System

We have juxtaposed the absolute ages and deformation amplitudes observed in Quaternary alluvial terraces over the structural seismic interpretation to quantify and date the horizontal displacements and slip rates associated with the Sosneado Thrust. To achieve this, we projected our seismic interpretations (Figure 7) and terrace

Table 2 – Analytical results summarizing the shortening, uplift and slip rates for each alluvial terrace of the Atuel River for the Sosneado Thrust. Only uplift rates are available for the folding above the Arroyo Blanco/La Manga thrust system because of the lack of subsurface characterization of the fault geometries. Average values (Q0-$T_{(i)}$) reflect the cumulative deformation of the alluvial terraces while incremental values ($T_{(i-1)}$-$T_{(i)}$) rather refers to the deformation between two deposition intervals.

Uplifted structures	Alluvial intervals	Time (ka)	Horizontal shortening (*V*) (m)	Shortening rates (mm.yr^{-1})	Vertical uplift (U) (m)	Uplift rates (mm.yr^{-1})	Slip on the Sosneado Thrust $r(x)$ (m)				Slip Rates on the Sosneado Thrust $S(x)$ (mm.yr^{-1})			
							r_1	r_2	r_3	r_4	S_1	S_2	S_3	S_4
Sosneado Thrust	Q0-Q2	11	10 ± 5	0.9 ± 0.6	6 ± 3	0.5 ± 0.3	11 ± 5.5	11 ± 5.5	12 ± 5.5	11 ± 5.5	1.0 ± 0.5	1.0 ± 0.5	1.1 ± 0.5	1.0 ± 0.5
	Q2-Q3	11	14 ± 4	1.3 ± 0.5	10 ± 3	0.9 ± 0.3	14 ± 4.2	16 ± 4.2	16 ± 4.2	16 ± 4.2	1.3 ± 0.4	1.5 ± 0.4	1.5 ± 0.4	1.5 ± 0.4
	Q0-Q3	22 ± 7	24 ± 5	1.1 ± 0.3	16 ± 3	0.7 ± 0.3	25 ± 9.2	27 ± 9.2	28 ± 9.2	27 ± 9.2	1.1 ± 0.4	1.2 ± 0.5	1.3 ± 0.5	1.2 ± 0.5
	Q3-Q4	49 ± 14	50 ± 6	1.0 ± 0.2	54 ± 6	1.1 ± 0.3	49 ± 14.4	49 ± 14.4	49 ± 14.4	49 ± 14.4	1.0 ± 0.3	1.0 ± 03	1.0 ± 0.3	1.0 ± 0.3
	Q0-Q4	71 ± 7	74 ± 3	1.0 ± 0.1	70 ± 3	1.1 ± 0.1	74 ± 8.0	76 ± 8.0	77 ± 8.0	76 ± 8.0	1.1 ± 0.1	1.1 ± 0.1	1.1 ± 0.1	1.1 ± 0.1
	Q4-Q5	4 ± 15	15 ± 23	3.7 ± 7.8	4 ± 3	1.0 ± 3.9	16 ± 63.8	16 ± 63.8	16 ± 63.8	16 ± 63.8	3.9 ± 15.7	3.9 ± 15.7	3.9 ± 15.7	3.9 ± 15.7
	Q0-Q5	75 ± 8	89 ± 4	1.2 ± 0.1	74 ± 3	1.1 ± 0.1	90 ± 10.3	92 ± 10.3	93 ± 10.3	92 ± 10.3	1.2 ± 0.1	1.2 ± 0.1	1.2 ± 0.1	1.2 ± 0.1
Arroyo Blanco/ La Manga thrusts	Q0-Q2	11	-	-	4 ± 3	0.4 ± 0.3	-	-	-	-	-	-	-	-
	Q0-Q3	22 ± 7	-	-	24 ± 3	1.1 ± 0.4	-	-	-	-	-	-	-	-
	Q0-Q4	71 ± 7	-	-	44 ± 3	0.6 ± 0.1	-	-	-	-	-	-	-	-

profiles (Figure 9) orthogonally with the Sosneado Thrust 's trace (Figure 16), similarly to section 10B. The uplift geometry of the main fault hanging wall cannot be balanced and restored by the fault bend fold model because we lack a structural reference frame in the footwall. The simple shear model has been used to estimate the displacement on the Sosneado Thrust (Figure 16A). Kinematic balancing is based on the principle of mass conservation and implies an increase in slip on the fault plane as its dip angle steepens and reconciles both horizontal and vertical displacement rates (*Bernard et al.*, 2007). This method has been successfully used to restore syn-sedimentary folded terraces in Central Taiwan (*Simoes et al.*, 2007). Cumulative horizontal shortening (*V*) and slip on the Sosneado Thrust (*r*) (Figure 16A) are estimated in section by area (*a*) balancing between the top of the deformed terraces and a theoretical paleo-river bed. For Q4 and Q5, the paleo-river bed is regarded as a straight line linking the tips of the folded terraces in the hanging wall of the fault (Figures 9C and 16B). For Q2 and Q3, since the tips of the fold are correlated with aggradational areas. i.e. buried beneath the present-day river bed, we use this latter as an approximated paleo-river bed. The displacements (*r(x)*) are calculated from four different segments (*x*) of the fault plane of varying dip angle ($\theta\ (x)$) (*Bernard et al.*, 2007):

$$r(x) = \frac{V.\sin(\psi)}{\sin(\psi - \theta(x))} \quad (1)$$

where ψ is the shear angle. V and r_1 are measured from the balanced area (a) for each terrace interval (Figure 16B), while $\theta(x)$ is measured from the seismic interpretation. The shear angle of the structure can be deduced from the equation (1):

$$\psi = \arctan\left(\frac{\sin\theta(1)}{\cos\theta(1) - \left(\frac{V}{r(1)}\right)}\right) \quad (2)$$

from which can be deduced the total and incremental slip rates ($S(x)$) for each segment of the fault plane.

This approach yields conservative estimates for the folded area as it does not consider folding in the footwall, as it may be also obscured by the accumulation of aggrading sediments in the footwall resulting from the morphodynamic response of the river to the uplift. Consequently, the values for r, V, and S should be regarded as minimal.

The profiles of Q2-Q4 are constrained by DEM data (Figure 10). The profile of Q5 was constructed using Q4 as a template (Figure 16B) and by generating a new horizon above it through kink bands. We adjusted this new horizon to fit with the remnants of the Q5 elevation profile.

The analytical results show that the cumulative horizontal shortening (*V*) ranges from 10 m (Q0-Q2) to 89 m (Q0-Q5), and the slip ($r(x)$) on the Sosneado Thrust ranges from 11 m (Q0-Q2) to 93 m (Q0-Q5) (Figure 17 and Table 2). The average shortening rates, based on the assigned ages of the markers range from 0.9 to 1.2 mm.yr^{-1} (Figure 18). The slip rates (S) range from 1.0 to 1.3 mm.yr^{-1}. The simple shear

	This study		Polanski (1963)	Baker et al. (2009)	
Age	Río Atuel (35°S) Alluvial surface	TCN Dating (ka)	Formations (Sosneado Area)	Río Diamante (34°33'S) Alluvial surface	Dating (ka)
HOLOCENE	Q_0	-	Los Alamitos	-	-
	Q_1	-			
PLEISTOCENE Upper	Q_2		El Zampal	Qt_5	13 ± 3
	Q_3	-	La Estacada	Qt_4	22 ± 7
	Q_4	71 ± 7	El Chilante	Qt_3	66 ± 14 69 ± 15
	Q_5	75 ± 8	El Tortoral	-	-
				-	-

Figure 15 – Stratigraphic correlation chart of the Río Atuel quaternary deposits. Ages of Q4 and Q5 (this work) were obtained from cosmogenic nuclide ^{10}Be and ^{26}Al technique (e.g. *Brown et al.*, 1991; *Brook et al.*, 1995; *Bierman et al.*, 1995; *Ritz et al.*, 1995; *Siame et al.*, 2000).

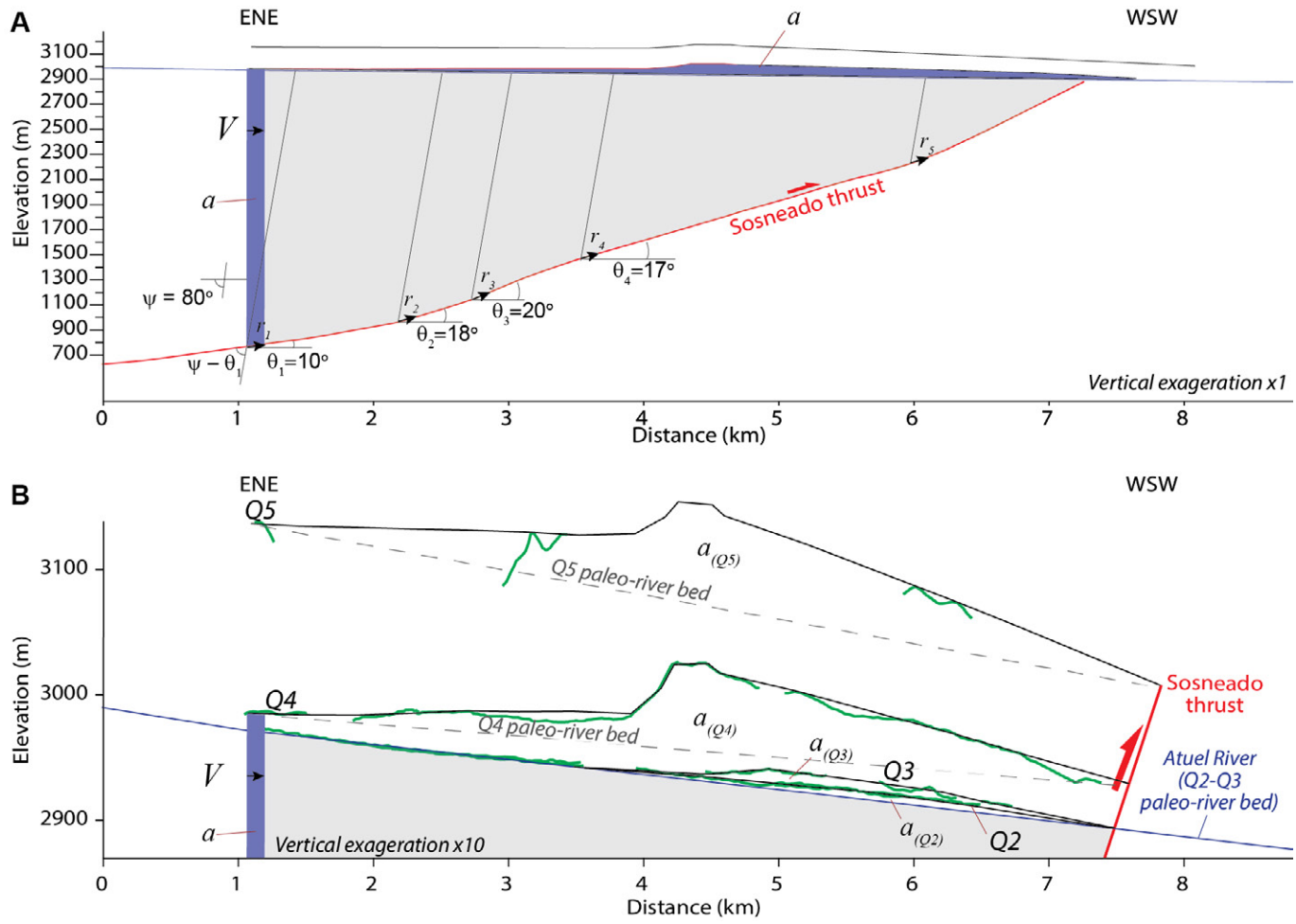

Figure 16 – **A-** Simplified cross section showing the relation between the horizontal shortening (V), the slip on the ramp (r), the ramp dip (θ) and the relative uplift area (a) above the ante-deformation river bed by simple shear deformation of the hanging wall (simple shear angle ψ). The conservation of the uplifted area gives the horizontal shortening implying that the slip varies along the ramp with the local dip (from *Bernard et al.*, 2007); **B-** Zoom-in of the Atuel River alluvial terraces (Q2 to Q5) above the Sosneado Thrust. (a) is the excess area above the ante-deformation paleo-river bed (dashed line). The green lines are raw topographic data extracted from the DEM. Q5 profile is reconstructed using Q4 as a template and aligning the profile dips with the alluvial remnants (using Move software; Petroleum Experts).

solution yields variations in displacements ranging from 1 to 3 m and slip rates in between 0.1 and 0.2 mm.yr^{-1} depending on the dip of the ramp segments. We remind that this calculation is free of the regional incision that occurred between Q5 and Q4.

The shortening and fault slip increments in between terraces in Q2-Q4 interval, are consistent and support both the ages and the deformation scenario of these terraces with a shortening rate of 1.0 mm.yr^{-1} (Table 2). Results on Q3-Q4 have the least uncertainties. Incremental results for Q4-Q5 are most uncertain as they deviate from the consistent shortening and slip trends obtained in the younger intervals (Table 2). One hypothesis to explain the trend deviation for Q5 may be due to an anomalous high shortening rate of ~15 m over 4 ka (3.7-3.9 mm.yr^{-1}, Table2 and Figure 18). Another alternative hypothesis is that the sparsity of exposed remnants of Q5 hamper accurate reconstructions of the terrace profile resulting in a wrong estimate of the folded area and therefore of the shortening values. For example, considering an age of 75 ka for Q5, the shortening overestimate reaches 11 m with respect to a shortening rate of 1.0 mm.yr^{-1} (Figure 18A). The grey area in Figure 18A displays the range of possible combinations of cumulative shortening and ages of Q5 that can fit an average Pleistocene slip rate of 1.0 mm.yr^{-1} and a Q4 age of 71 ka. Considering the minimum and maximum ages of 67 ka and 83 ka for Q5, respectively determined by the uncertainties in the TCN dating, and considering that Q5 cannot be less deformed than Q4, the cumulative shortening recorded by Q5 falls within the range of 74 and 88 m (Figure 18A).

The structural restoration of the terraces consolidates our results on Q2-Q4 (Figure 19A-C). This restoration based on simple shear unfaulting and unfolding, with a shear angle and fault heaves deduced from analytical results, indicates paleo-river beds that consistently restore below the current river level. This suggests that without tectonic uplift above the Sosneado Thrust, the successive alluvial systems would be aggrading. This is consistent with the sedimentary aggradation observed downstream

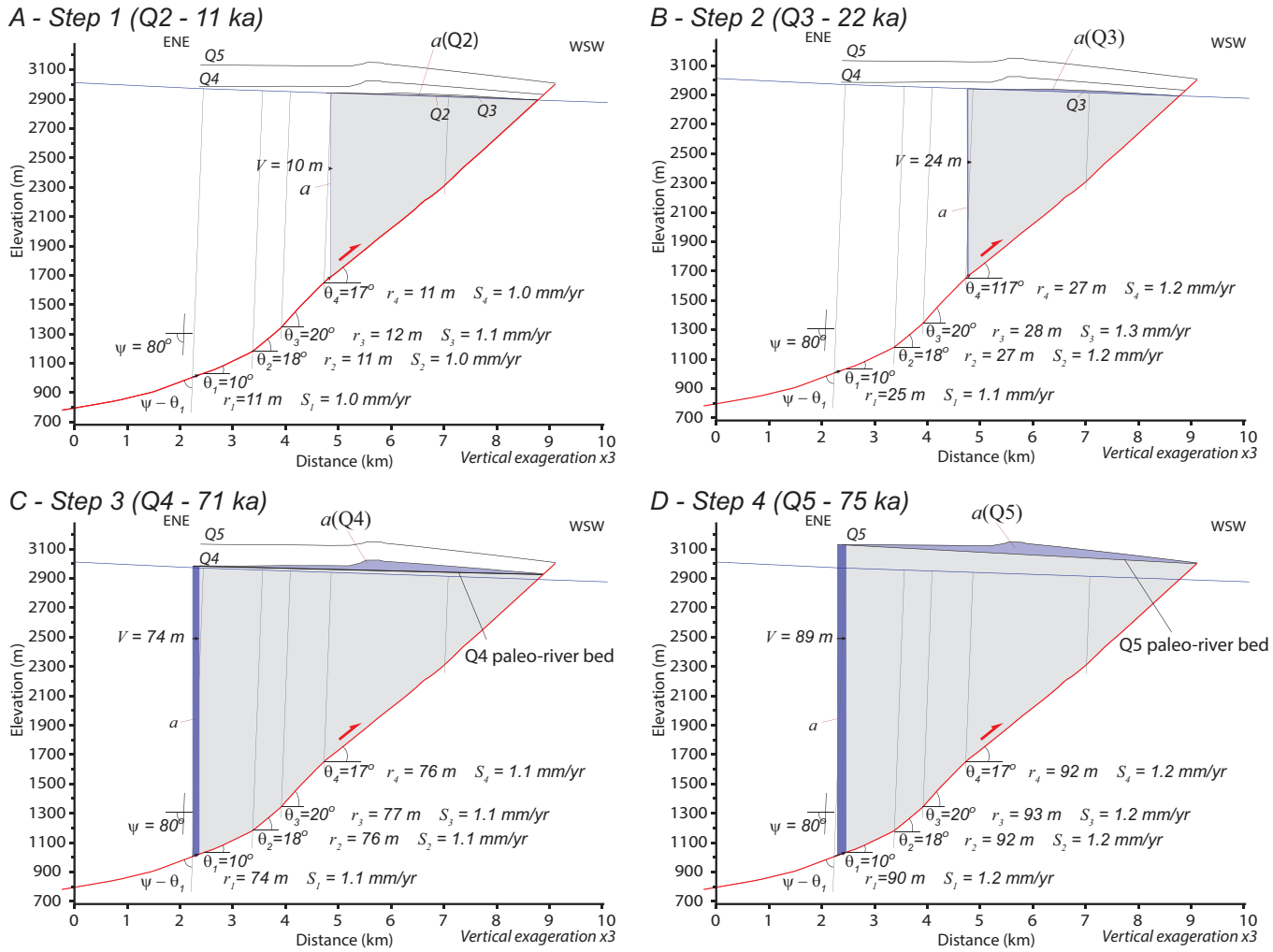

Figure 17 – Average slip displacement and rates deduced for each ramp segment for Q2 **(A)**, Q3 **(B)**, Q4 **(C)** and Q5 **(D)**. The conservation of the measured uplifted area (*a* – light blue area of an initially undeformed paleo-river bed, allows estimating the total horizontal shortening (*V* – width of the dark blue area) and variable slip displacements ($r_{(1-4)}$) and rates ($S_{(1-4)}$) along the ramp segments.

of the frontal ridge.

Considering our tentative reconstruction for Q5, which accounts for a cumulative shortening of 89 m over 75 ka, the incremental shortening, and consequently the fault heave, amounts to 15 m (Table 2 and Figure 18B). The restored paleo-river bed is approximately 89 m higher than Q4 in the footwall of the Sosneado Thrust (scenario Sc1 in Figure 19D). Alternatively, the minimum and maximum age uncertainties of the TCN dating, respectively for Q4 (63 ka) and Q5 (83 ka), allows the estimation of the maximum potential incremental horizontal shortening in between Q5 and Q4, assuming a constant shortening rate of 1.2 mm.yr^{-1} (Figure 18B). This yields a maximum possible fault heave for Q5 restoration of 22 m (Figure 18B and 19D). The restored paleo-river for Q5 would stand 83 meters above the paleo-river bed of Q4 (Scenario Sc2 in Figure 19D). The magnitude of this residual incision is contingent upon the uncertainties in age difference between Q4 and Q5, ranging from 4 ka (Sc1) to 20 ka (Sc2). The rate of incision reaches 22 mm.yr^{-1} for Sc1 and 4 mm.yr^{-1} for Sc2. The slope of the restored Q5 surface is 2.4%, significantly higher than the ~1.1% of the present-day and Q1-Q4 restored river beds (Figure 19D).

The high incision rate from Q5 to Q4, found all over the study area (Figure 9B) cannot be attributed to tectonic folding. The steep slope of the restored Q5 surface suggests either the deposition of an alluvial fan, and/or a transient river adjustment to local hydrological changes that occurred between 70 and 80 ka. The sub-stage fluctuations associated with the interglacial and glacial periods within Marine Isotope Stage 5 (MIS5), occurring every 5-10 kyr (*Lisiecki and Raymo*, 2005), may have been influential. Conversely, Q4 appears to be associated with a significant aggradational event that occurred during the glacial episode of MIS 4, dated to 57-71 ka (*Baker et al.*, 2009). Additionally, autogenic processes such as reorganization of watersheds and river captures may have played a role in the incision, although the precise mechanisms behind these processes remain unknown.

Further upstream, at the southern tip of the Arroyo Blanco and La Manga thrusts, the tectonic uplift

rates, evidenced by the difference in height between the top of the abandoned alluvial terraces and their theorical undeformed paleo-river bed (Figure 10A), are similar to the rates estimated for the Sosneado Thrust (Table 2). Total uplift relative to Q0 reaches 4 m for Q2, 24 m for Q3 and 44 m for Q4. This gives uplift rates of 0.4 ± 0.3 mm.yr^{-1} for the interval Q0-Q2, 1.1 ± 0.4 mm.yr^{-1} for the interval Q0-Q3 and 0.6 ± 0.1 mm.yr^{-1} for the interval Q0-Q4. These results are free of the regional incision that occurred between Q5 and Q4). Shortening and slip rates cannot be estimated due to a lack of a reliable structural interpretation in the subsurface (seismic data).

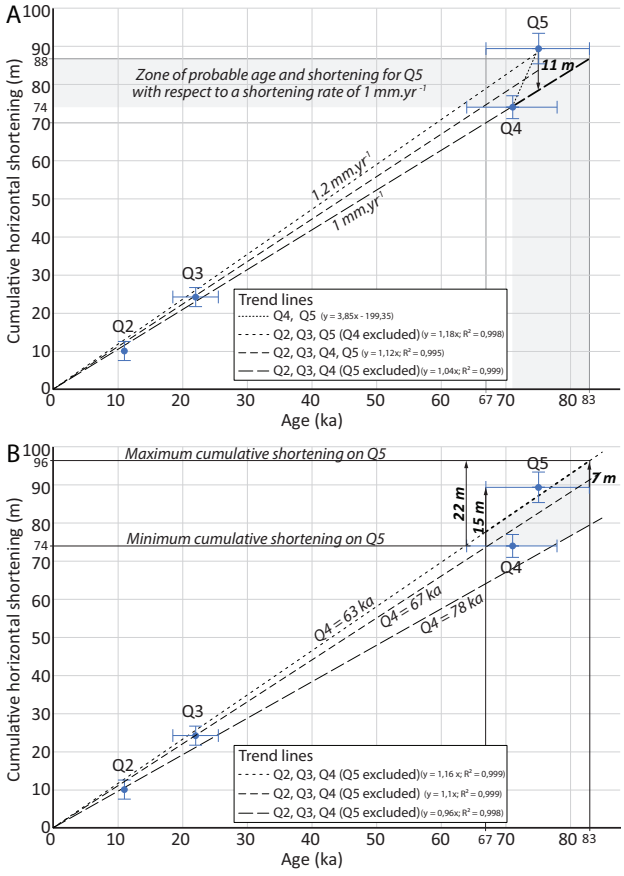

Figure 18 – Cumulative horizontal shortening vs. age of alluvial terrace. **A-** The grey area delineates the probable age zone and the cumulative shortening relative to a constant shortening rate of 1 mm.yr^{-1}, which represents the optimal fit when considering only Q2, Q3, and Q4. Under these conditions, reconstructing Q5 would result in a mismatch, leading to an overestimation of the cumulative shortening by 11 meters in Q5.; **B-** The age and cumulative shortening, as inferred from the constant shortening rates corresponding to the youngest and oldest estimated ages of Q4 (63-78 ka), are constrained by the uncertainties associated with the TCN dating. We assume that the uncertain reconstruction of the Q5 profile is potentially inaccurate. The grey area represents the range of possible age and cumulative shortening scenarios for Q5. If Q4 is as young as 63 ka and Q5 is as old as 83 ka, the maximum incremental shortening occurring between Q4 and Q5 reaches 22 m, suggesting that the overall calculated cumulative shortening might be underestimated by up to 7 m.

8.3 New insights on hazardous fault systems at 35°S

The total displacement along the Sosneado Thrust over approximately 9 Myr, which is the age of the thrust initiation according to *Giambiagi et al.* (2008), is estimated at ~1500 m. This indicates an average shortening rate of only ~0.16 mm.yr^{-1} since the Lower Miocene, about 7 times smaller than the shortening rates recorded in the late Pleistocene (Table 2). This suggests that the southern segment of the Sosneado Thrust has been active during the Pleistocene, concomitantly with the compression recorded around the southern tip of the La Manga Thrust. Consequently, the thrust front of the Malargüe FTB although not mapped as a hazardous fault zone in South America (*Costa et al.*, 2020), is the locus of seriously unreported recent faulting, worth considering in future seismic risks evaluations. Moreover, these observations are significant because they were made only 40 km north of Malargüe, a town with a population of 27,000 (Figure 1A and B).

Most earthquakes with magnitudes greater than 7 in the Andean retro-arc broken foreland occur along deep crustal faults. Deeper crustal faults are more prone to accumulating stress and sourcing larger seismic events than shallower faults dissecting sedimentary rock. Deformation seen at the thin-skinned thrust front of the Malargüe FTB likely represents the shallower accommodation of slip on deep-seated crustal thrusts at the edge of the Principal Cordillera. The more rigid, thick-skinned front of the Malargüe FTB is predisposed to localizing the most substantial earthquakes (Figure 2). Thus, the La Manga and Arroyo Blanco faults should be regarded as presenting higher seismic hazards, while the Sosneado Thrust is expected to absorb a share of the co-seismic displacement occurring in the thin-skinned region. Additional displacement must also be considered for concomitant thin-skinned structures identified along the Arroyo Blanco and La Manga thrusts (see the uplift rate magnitudes on Table 2), as well as any other Quaternary structures like the Mesón and Alquitrán thrusts situated to the north of the Atuel River (Figure 2). Consequently, the horizontal shortening rate along the deep crustal thrust at 35°S is likely to be at least equal or larger than the rate of 1.1 mm.yr^{-1} recorded on the Sosneado Thrust.

The estimated shortening rates at the thick-skinned front of the Malargüe FTB at 36°S for the Pliocene to middle Pleistocene time interval are comparable, with values of 1.1 mm.yr^{-1} reported for the Malargüe Anticline and 0.4 mm.yr^{-1} reported for the Chacay Anticline (*Lopasso et al.*, 2024). Shortening rates of similar magnitudes have been also reported from the better-studied areas in between 31 and 33°S, where relationships between faults and earthquakes have been established. For example, in the Eastern Precordillera near the city of San Juan (31.5°S; SJ in Figure 1A), *Rockwell et al.* (2014) and *Siame et al.*

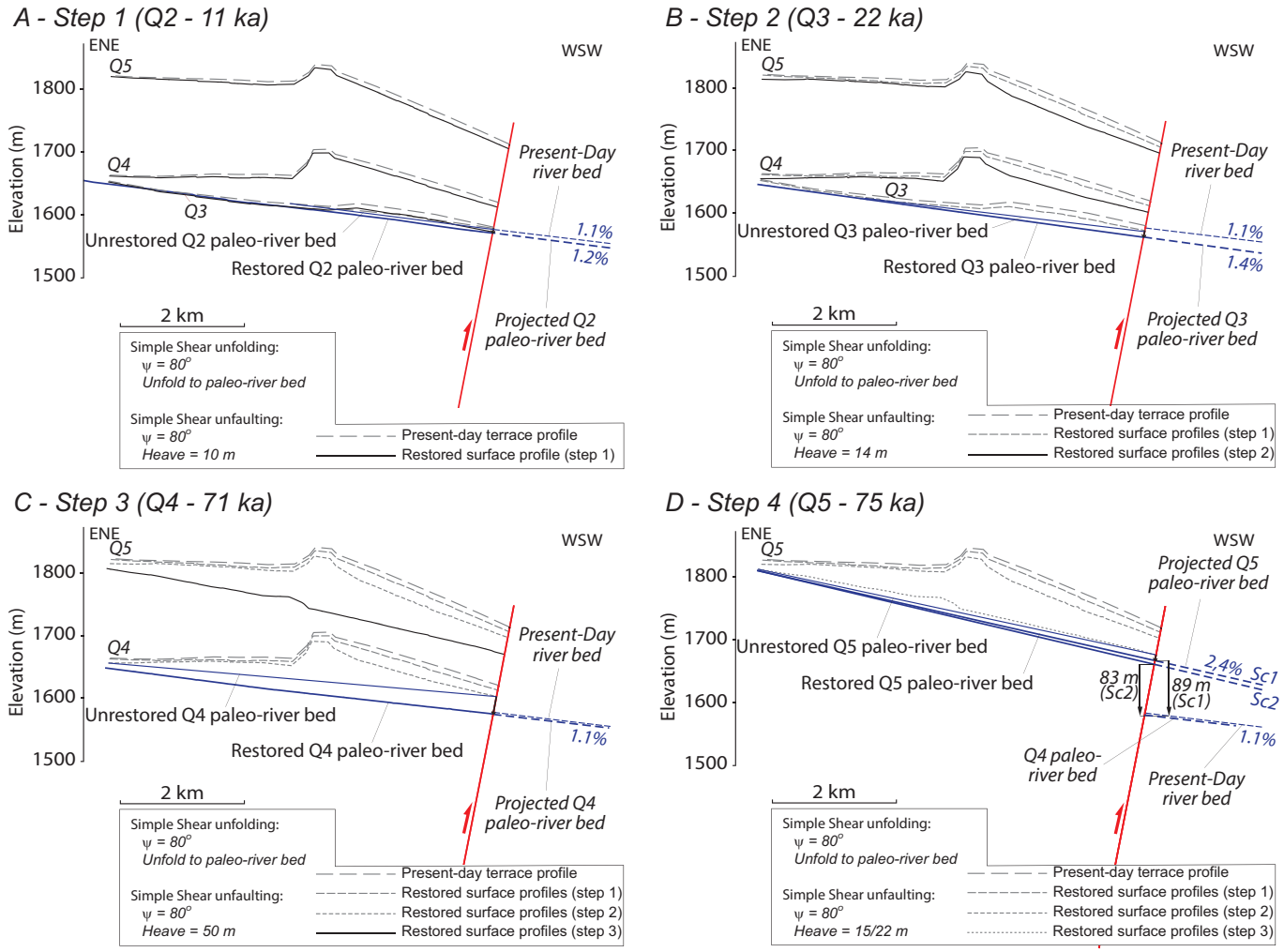

Figure 19 – Incremental structural restoration of terrace profiles using Move software (Petroleum Experts). The equation used is simple shear unfolding followed by simple shear unfaulting, with a shear angle (ψ) of 80° and incremental horizontal shortening (fault heave) obtained from analytical results herein. The dashed lines represent the restored terraces' profiles according to the step restoration of the younger intervals. In (D), Sc1 and Sc2 refer to two possible scenarios for the restoration. Sc1: Q4 and Q5 have ages of 71 and 75 ka with a difference in age of 4 ka. The corrected incremental horizontal shortening in between Q5 and Q4 with respect to a theoritical shortening rate of 1.0 mm.yr^{-1} would be 4 m (Figure 18A). Sc2: we consider the minimum and maximum uncertainties of the TCN dating for Q4 (63 ka) and Q5 (83 ka). The maximum incremental horizontal shortening between Q5 and Q4 is 22 m (Figure 18B).

(2002) estimated slip rates of 0.8 mm.yr^{-1} along an east-dipping thin-skinned secondary fault of the Villicum thrust system and 1.1 mm.yr^{-1} along the east-verging crustal La Laja Fault, locus of the Mw 7 La Laja earthquake on January 1944 (Figure 1C). Approximately 40 km to the east, along the Sierras Pampeanas ranges, the eastern Sierra de Pie de Palo thick-skinned fault locus of the Mw 7.4 earthquake (1977) has a slip rate estimated at 0.5 mm.yr^{-1} by *Siame et al.* (2015) (Figure 1C). Similar earthquake magnitudes (Mw 6.8-7.4) have been tied to crustal faults in the easternmost region of the broken foreland, with slip rate estimates ranging from ~0.01-0.36 mm.yr^{-1} (Sierra Chica; *Costa et al.*, 2021) to 2 mm.yr^{-1} (Sierra Comechingones; *Costa and Finzi*, 1996) (Figure 1C). Along the Precordillera thrust front, further south, near the city of Mendoza (Me in Figure 1A), the shortening rate of the Peñas Fault is estimated in between 0.3 and 2 mm.yr^{-1} (*Schmidt et al.*, 2011; *Costa et al.*, 2019), while the Cal fault, locus of for the Ms 7 earthquake that destroyed Mendoza in 1861, has a shortening rate estimated in between 1.5 and 5.4 mm.yr^{-1} (*Schmidt et al.*, 2011).

The style of deformation is similar throughout the region, and if we consider the studies carried out in the north on seismicity (historical and instrumental) and length of Andean thrusts, earthquakes of magnitude 6 to 7 may be expected along the border faults of the main Cordillera. However, considering the slip rates of the faults, the recurrence times of major earthquakes are likely to be several hundred years. Therefore, the current instrumental and historical seismicity catalogs are unlikely to account for all seismic hazards of the region. Thus, it would be reasonable to conduct more detailed palseoseismic investigations in the region to better constrain coseismic displacements and thoroughly monitor tectonic activity.

Our results infirm the claim that seismic hazards

south of the Pampean flat slab are much lower due to decreased plate coupling and a less intense back-arc shortening in the region after the Miocene. Regardless of the underlying subducting slab's geometry, the structural processes leading to active deformation are similar throughout the whole region and seismic hazards are significant. Assuming that an underlying slab steepening leads to minimal active and seismic deformation in back-arc regions is not backed by our results. Temporary local seismic stations record crustal earthquakes of magnitudes up to 5, as south as 38°S ,in the broken foreland of the Neuquén Andes, some 200 km east of the thrust front of the Principal Cordillera (Figure 1A; *Messager et al.*, 2023).

9 Conclusion

We performed detailed mapping of five alluvial terraces (Q1-Q5) bracketing the Atuel River across the Malargüe FTB at 35°S along the Andean Principal Cordillera of Argentina. New TCN dating of surfaces atop deposits of Q4 and Q5 terraces gives yield ages of 71 and 75 ka. The analysis of their incision and residual topographic longitudinal profiles have led to identify at the front of the Malargüe Fold-and-Thrust Belt two 7 km-wide gradual uplifts during the late Pleistocene to Holocene; both around the southern tip of the Arroyo Blanco and La Manga thick-skinned thrusts, and above the Sosneado thin-skinned thrust. In addition, field observations provided evidence for thrusting and folding within the Atuel River's alluvial terraces and adjacent Quaternary deposits in the hanging wall of the Sosneado Thrust, attesting for its activity during the late Pleistocene.

The cumulative folding of the Atuel River's alluvial terrace remnants over a duration of 75 ka best approximates the behavior of the Sosneado Thrust during the late Pleistocene, implying a shortening rate of 0.9-1.2 $\pm$ 0.3 mm.yr^{-1} and a slip rate on the ramp of 1.0-1.3 $\pm$ 0.2 mm.yr^{-1}. The restoration of a seismic section across the mountain front back to a Miocene pre-growth step, yields a significantly slower shortening rate for this 9 Ma long time interval. This suggests that the Malargüe Fold-and-Thrust Belt front mainly developed during the Quaternary, hence recording a late eastward migration of the deformation front.

The similarities between the structural styles and kinematics of the seismogenic crustal faults within the Malargüe FTB, and those in the Pampean flat slab region at 33°S, suggest that earthquakes with magnitudes of 6 to 7 are plausible along the faults bordering the Principal Cordillera at 35°S. Therefore, despite the recent focus for seismic risks being concentrated further East on the San Rafael Block due to historical destructive events, the potential for seismogenic hazards along the eastern border of the Andean Principal Cordillera should also be closely monitored at these latitudes. Our results contest the prevailing view that seismic hazards are marginal south of the Pampean flat slab area due to weaker plate coupling and reduced back-arc shortening since the Pliocene.

Acknowledgements

We express our gratitude to Total SA for generously providing funding for the fieldwork, data access, sampling, and analysis. We thank Martine Simoes and Carlos Costa for their invaluable reviews which have significantly improved the original manuscript. We also thank the editors Robin Lacassin and Jack Williams for their additional comments. We extend our special appreciation to Jean-Paul Xavier (Total ASA) and Pr. Yves Hervouët (University of Pau) for their invaluable support and meaningful discussions. ASTER AMS, national facility (CEREGE, Aix en Provence), is supported by the INSU/CNRS and IRD and member of AIX MARSEILLE PLATFORMS and REGEF networks.

Author contributions

Grégoire Messager was involved in project conceptualization, investigation, data interpretation, and formal analysis, and supervised the writing process. **Bertrand Nivière** contributed to project conceptualization and investigation. **Pierre Lacan** has been contributing to the investigation, **Vincent Regard** to the TCN dating, and **Eric Blanc** to the structural seismic interpretation and restoration. **BN**, **PL**, **VR** and **EB** all proofread and provided critical revisions to the manuscript and were also involved in the writing.

Data availability

Landsat 7 images are available on the USGS website (www.usgs.gov/landsat-missions/landsat-7). ASTER images and their derivative GDEMs are accessible at no cost on the JPL NASA website (www.asterweb.jpl.nasa.gov). 2D seismic reflection and borehole data were kindly provided by Total ASA. The earthquake catalogs can be freely downloaded from the USGS (www.earthquake.usgs.gov/earthquakes) and INPRES (www.inpres.gob.ar) catalogs. Information on the crustal present-day stress field is accessible for free on the World Stress Map dataset website (www.world-stress-map.org). TCN dating of alluvial terraces are in one part, obtained from duly referenced previous studies, and in the other part, obtained from our own TCN dating analysis and results and reported in the tables S1, S2, and S3 of the Supporting Information.

Competing interests

The authors declare no competing interests.

Peer review

This publication was peer-reviewed by Carlos Costa and Martine Simoes. The full peer-review report can be found here: tektonika.online/index.php/home/article/view/63/101

Copyright notice

References

Allmendinger, R. W., D. Figueroa, D. Snyder, J. Beer, C. Mpodozis, and B. L. Isacks (1990), Foreland shortening and crustal balancing in the Andes at 30°S latitude, *Tectonics*, *9*, 789–809, doi: 10.1029/TC009i004p00789.

Alvarado, P., and S. Beck (2006), Source characterization of the San Juan (Argentina) crustal earthquakes of 15 January 1944 (Mw 7.0) and 11 June 1952 (Mw 6.8), *Earth and planetary science letters*, *243*(3), 615–631, doi: 10.1016/j.epsl.2006.01.015.

Alvarado, P., S. Beck, G. Zandt, M. Araujo, and E. Triep (2005), Crustal deformation in the south-central Andes backarc terranes as viewed from regional broad-band seismic waveform modelling, *Geophysical Journal International*, *163*(2), 580–598, doi: 10.1111/j.1365-246X.2005.02759.x.

Anderson, M., P. Alvarado, G. Zandt, and S. Beck (2007), Geometry and brittle deformation of the subducting Nazca Plate, Central Chile and Argentina, *Geophysical Journal International*, *171*(1), 419–434, doi: 10.1111/j.1365-246X.2007.03483.x.

Anderson, R. S., J. L. Repka, and G. S. Dick (1996), Explicit treatment of inheritance in dating depositional surfaces using in situ 10Be and 26Al, *Geology*, *24*(1), 47–51, doi: 10.1130/0091-7613(1996)024<0047:ETOIID>2.3.CO;2.

Astini, R. A. (1998), Stratigraphical evidence supporting the rifting, drifting and collision of the Laurentian Precordillera terrane of western Argentina, *Geological Society, London, Special Publications*, *142*(1), 11–33, doi: 10.1144/GSL.SP.1998.142.01.02.

Baker, S. E., J. C. Gosse, E. V. McDonald, E. B. Evenson, and O. Martínez (2009), Quaternary history of the piedmont reach of Río Diamante, Argentina, *Journal of South American Earth Sciences*, *28*(1), 54–73, doi: 10.1016/j.jsames.2009.01.001.

Balco, G., J. O. Stone, N. A. Lifton, and T. J. Dunai (2008), A complete and easily accessible means of calculating surface exposure ages or erosion rates from 10Be and 26Al measurements, *Quaternary geochronology*, *3*(3), 174–195, doi: 10.1016/j.quageo.2007.12.001.

Bande, A., A. Boll, F. Fuentes, B. K. Horton, and D. F. Stockli (2020), Thermochronological Constraints on the Exhumation of the Malargüe Fold-Thrust Belt, Southern Central Andes, in *Opening and Closure of the Neuquén Basin in the Southern Andes*, vol. Not available, edited by D. Kietzmann and A. Folguera, pp. 371–396, Springer International Publishing, Cham, doi: 10.1007/978-3-030-29680-3_15.

Bechis, F., L. Giambiagi, V. García, S. Lanés, E. Cristallini, and M. Tunik (2010), Kinematic analysis of a transtensional fault system: The Atuel depocenter of the Neuquén basin, southern Central Andes, Argentina, *Journal of Structural Geology*, *32*(7), 886–899, doi: 10.1016/j.jsg.2010.03.009.

Bernard, S., J. Avouac, S. Dominguez, and M. Simoes (2007), Kinematics of fault-related folding derived from a sandbox experiment, *Journal of Geophysical Research, [Solid Earth]*, *112*, Not available, doi: 10.1029/2005JB004149.

Bierman, P. R. (1994), Using in situ produced cosmogenic isotopes to estimate rates of landscape evolution: A review from the geomorphic perspective, *Journal of Geophysical Research, [Solid Earth]*, *99*, 13,885–13,896, doi: 10.1029/94JB00459.

Bierman, P. R., A. R. Gillespie, and M. W. Caffee (1995), Cosmogenic Ages for Earthquake Recurrence Intervals and Debris Flow Fan Deposition, Owens Valley, California, *Science*, *270*(5235), 447–450, doi: 10.1126/science.270.5235.447.

Branellec, M., B. Nivière, J.-P. Callot, V. Regard, and J.-C. Ringenbach (2016a), Evidence of active shortening along the eastern border of the San Rafael basement block: characterization of the seismic source of the Villa Atuel earthquake (1929), Mendoza province, Argentina, *Geological magazine*, *153*(5-6), 911–925, doi: 10.1017/S0016756816000194.

Branellec, M., B. Nivière, J.-P. Callot, and J.-C. Ringenbach (2016b), Mechanisms of basin contraction and reactivation in the basement-involved Malargüe fold-and-thrust belt, Central Andes (34–36°S), *Geological magazine*, *153*(5-6), 926–944, doi: 10.1017/S0016756816000315.

Brook, E. J., E. T. Brown, M. D. Kurz, R. P. Ackert, G. M. Raisbeck, and F. Yiou (1995), Constraints on age, erosion, and uplift of Neogene glacial deposits in the Transantarctic Mountains determined from in situ cosmogenic 10Be and 26Al, *Geology*, *23*(12), 1063–1066, doi: 10.1130/0091-7613(1995)023<1063:COAEAU>2.3.CO;2.

Brooks, B. A., M. Bevis, R. Smalley, Jr, E. Kendrick, R. Manceda, E. Lauría, R. Maturana, and M. Araujo (2003), Crustal motion in the Southern Andes (26°–36°S): Do the Andes behave like a microplate?, *Geochemistry, Geophysics, Geosystems*, *4*(10), Not available, doi: 10.1029/2003gc000505.

Brown, E. T., J. M. Edmond, G. M. Raisbeck, F. Yiou, M. D. Kurz, and E. J. Brook (1991), Examination of surface exposure ages of Antarctic moraines using in situ produced 10Be and 26Al, *Geochimica et cosmochimica acta*, *55*(8), 2269–2283, doi: 10.1016/0016-7037(91)90103-C.

Brown, E. T., R. F. Stallard, M. C. Larsen, G. M. Raisbeck, and F. Yiou (1995), Denudation rates determined from the accumulation of in situ-produced 10Be in the luquillo experimental forest, Puerto Rico, *Earth and planetary science letters*, *129*(1), 193–202, doi: 10.1016/0012-821X(94)00249-X.

Cande, S. C., and R. B. Leslie (1986), Late Cenozoic tectonics of the southern Chile Trench, *Journal of geophysical research*, *91*(B1), 471–496, doi:

10.1029/jb091ib01p00471.

Cerling, T. E., and H. Craig (1994), GEOMORPHOLOGY AND IN-SITU COSMOGENIC ISOTOPES, *Annual review of earth and planetary sciences*, *22*(Volume 22, 1994), 273–317, doi: 10.1146/annurev.ea.22.050194.001421.

Charrier, R., L. Pinto, and M. P. Rodríguez (2007), Tectonostratigraphic evolution of the Andean Orogen in Chile, in *The Geology of Chile*, Geological Society of London, doi: 10.1144/GOCH.3.

Chernicoff, C. J., and E. O. Zappettini (2004), Geophysical Evidence for Terrane Boundaries in South-Central Argentina, *Gondwana Research*, *7*(4), 1105–1116, doi: 10.1016/S1342-937X(05)71087-X.

Cobbold, P. R., and E. A. Rossello (2003), Aptian to recent compressional deformation, foothills of the Neuquén Basin, Argentina, *Marine and Petroleum Geology*, *20*(5), 429–443, doi: 10.1016/S0264-8172(03)00077-1.

Colavitto, B., L. Sagripanti, L. Fennell, A. Folguera, and C. Costa (2019), Evidence of Quaternary tectonics along Río Grande valley, southern Malargüe fold and thrust belt, Mendoza, Argentina, *Geomorphology*, *346*, 106,812, doi: 10.1016/j.geomorph.2019.06.025.

Cominguez, A. H., and V. A. Ramos (1991), LA ESTRUCTURA PROFUNDA ENTRE PRECORDILLERA y SIERRAS PAMPEANAS DE LA ARGENTINA: EVIDENCIAS DE LA SISMICA DE REFLEXION PROFUNDA, *Andean Geology*, *18*, 3–14, doi: 10.5027/ANDGEOV18N1-A01.

Costa, C., H. Cisneros, J. Salvarredi, and A. Gallucci (2006), La neotectónica del margen oriental del bloque de San Rafael: Nuevas consideraciones, *Asociación Geológica Argentina, Serie D: Publicación Especial*, *6*, 33–40.

Costa, C., A. Alvarado, F. Audemard, L. Audin, C. Benavente, F. H. Bezerra, J. Cembrano, G. González, M. López, E. Minaya, I. Santibañez, J. Garcia, M. Arcila, M. Pagani, I. Pérez, F. Delgado, M. Paolini, and H. Garro (2020), Hazardous faults of South America; compilation and overview, *Journal of South American Earth Sciences*, *104*, 102,837, doi: 10.1016/j.jsames.2020.102837.

Costa, C. H., and C. V. Finzi (1996), Late Holocene faulting in the southeast Sierras Pampeanas of Argentina, *Geology*, *24*(12), 1127–1130, doi: 10.1130/0091-7613(1996)024<1127:LHFITS>2.3.CO;2.

Costa, C. H., L. M. Schoenbohm, B. A. Brooks, C. E. Gardini, and A. D. Richard (2019), Assessing Quaternary shortening rates at an Andean frontal thrust (32°30'S), Argentina, *Tectonics*, *38*(8), 3034–3051, doi: 10.1029/2019tc005564.

Costa, C. H., L. A. Owen, W. J. Johnson, and E. Kirby (2021), Quaternary activity and seismogenic potential of the Sierra Chica Fault System, Pampean Ranges of Argentina, *Journal of South American Earth Sciences*, *110*, 103,328, doi: 10.1016/j.jsames.2021.103328.

del Papa, C., F. Hongn, J. Powell, P. Payrola, M. Do Campo, M. R. Strecker, I. Petrinovic, A. K. Schmitt, and R. Pereyra (2013), Middle Eocene-Oligocene broken-foreland evolution in the Andean Calchaqui Valley, NW Argentina: insights from stratigraphic, structural and provenance studies, *Basin Research*, *25*(5), 574–593, doi: 10.1111/bre.12018.

Desilets, D., and M. Zreda (2003), Spatial and temporal distribution of secondary cosmic-ray nucleon intensities and applications to in situ cosmogenic dating, *Earth and planetary science letters*, *206*(1), 21–42, doi: 10.1016/S0012-821X(02)01088-9.

Desilets, D., M. Zreda, and T. Prabu (2006), Extended scaling factors for in situ cosmogenic nuclides: New measurements at low latitude, *Earth and planetary science letters*, *246*(3), 265–276, doi: 10.1016/j.epsl.2006.03.051.

Dunai, T. J. (2001), Influence of secular variation of the geomagnetic field on production rates of in situ produced cosmogenic nuclides, *Earth and planetary science letters*, *193*(1), 197–212, doi: 10.1016/S0012-821X(01)00503-9.

Dávila, F. M., and R. A. Astini (2003), Early Middle Miocene broken foreland development in the southern Central Andes: evidence for extension prior to regional shortening, *Basin Research*, *15*(3), 379–396, doi: 10.1046/j.1365-2117.2003.00206.x.

Dávila, F. M., M. E. Giménez, J. C. Nóbile, and M. P. Martínez (2012), The evolution of the high-elevated depocenters of the northern Sierras Pampeanas (*ca*. 28˚ SL), Argentine broken foreland, South-Central Andes: the Pipanaco Basin, *Basin Research*, *24*(6), 615–636, doi: 10.1111/j.1365-2117.2011.00539.x.

Folguera, A., J. A. Naranjo, Y. Orihashi, H. Sumino, K. Nagao, E. Polanco, and V. A. Ramos (2009), Retroarc volcanism in the northern San Rafael Block (34°–35°30'S), southern Central Andes: Occurrence, age, and tectonic setting, *Journal of Volcanology and Geothermal Research*, *186*(3), 169–185, doi: 10.1016/j.jvolgeores.2009.06.012.

Folguera, A., G. Gianni, L. Sagripanti, E. Rojas Vera, I. Novara, B. Colavitto, O. Alvarez, D. Orts, J. Tobal, M. Giménez, A. Introcaso, F. Ruiz, P. Martínez, and V. A. Ramos (2015), A review about the mechanisms associated with active deformation, regional uplift and subsidence in southern South America, *Journal of South American Earth Sciences*, *64*, 511–529, doi: 10.1016/j.jsames.2015.07.007.

Franzese, J. R., and L. A. Spalletti (2001), Late Triassic–early Jurassic continental extension in southwestern Gondwana: tectonic segmentation and pre-break-up rifting, *Journal of South American Earth Sciences*, *14*(3), 257–270, doi: 10.1016/S0895-9811(01)00029-3.

Fuentes, F., B. K. Horton, D. Starck, and A. Boll (2016), Structure and tectonic evolution of hybrid thick- and thin-skinned systems in the Malargüe fold–thrust belt, Neuquén basin, Argentina, *Geological magazine*, *153*(5-6), 1066–1084, doi: 10.1017/S0016756816000583.

Galland, O., E. Hallot, P. R. Cobbold, G. Ruffet, and J. de Bremond d'Ars (2007), Volcanism in a compressional Andean setting: A structural and geochronological study of Tromen volcano (Neuquén province, Argentina), *Tectonics*, *26*, Not available, doi: 10.1029/2006TC002011.

Galland, O., H. J. Villar, J. Mescua, D. A. Jerram, G. Messager, A. Medialdea, I. Midtkandal, J. O. Palma, S. Planke, L. E. Augland, and A. Zanella (2024), Structural control of igneous intrusions on fluid migration in sedimentary basins: the case study of large bitumen seeps at Cerro Alquitrán and Cerro La Paloma, northern Neuquén Basin, Argentina, *Geological Society, London, Special Publications*, *547*(1), SP547–2023–115, doi: 10.1144/SP547-2023-115.

García Morabito, E., A. Beltrán-Triviño, C. M. Terrizzano, F. Bechis, J. Likerman, A. Von Quadt, and V. A. Ramos (2021), The influence of climate on the dynamics of mountain building within the northern Patagonian Andes, *Tectonics*, *40*(2), Not available, doi: 10.1029/2020tc006374.

Giambiagi, L., F. Bechis, V. García, and A. H. Clark (2008), Temporal and spatial relationships of

thick- and thin-skinned deformation: A case study from the Malargüe fold-and-thrust belt, southern Central Andes, *Tectonophysics*, *459*(1), 123–139, doi: 10.1016/j.tecto.2007.11.069.

Giambiagi, L. B., M. A. Tunik, and M. Ghiglione (2001), Cenozoic tectonic evolution of the Alto Tunuyán foreland basin above the transition zone between the flat and normal subduction segment (33°30'–34°S), western Argentina, *Journal of South American Earth Sciences*, *14*(7), 707–724, doi: 10.1016/S0895-9811(01)00059-1.

Gimenez, M. E., M. P. Martínez, and A. Introcaso (2000), A crustal model based mainly on gravity data in the area between the Bermejo Basin and the Sierras de Valle Fértil, Argentina, *Journal of South American Earth Sciences*, *13*(3), 275–286, doi: 10.1016/S0895-9811(00)00012-2.

González-Díaz, E. (1964), Rasgos geológicos y evolución geomorfológica de la Hoja 27 d (San Rafael) y zona occidental vecina (Provincia de Mendoza), *Revista de la Asociación Geológica Argentina*, *19*(3), 151–188.

Gosse, J. C. (1994), Alpine glacial history reconstruction: 1. Application of the cosmogenic beryllium-10 exposure age method to determine the glacial chronology of the Wind River Mountains, Wyoming, United States of America. 2. Relative dating of Quaternary deposits in the Rio Atuel Valley, Mendoza, Argentina, Ph.D. thesis, Lehigh University, Bethlehem, PA, USA.

Granger, D. E., and P. F. Muzikar (2001), Dating sediment burial with in situ-produced cosmogenic nuclides: theory, techniques, and limitations, *Earth and planetary science letters*, *188*(1), 269–281, doi: 10.1016/S0012-821X(01)00309-0.

Gregori, S. D., and R. Christiansen (2018), Seismic hazard analysis for central-western Argentina, *Geodesy and Geodynamics*, *9*(1), 25–33, doi: 10.1016/j.geog.2017.07.006.

Groeber, P. (1929), Líneas fundamentales de la geología del Neuquén, sur de Mendoza y regiones adyacentes, *Tech. rep.*, Ministerio de Agricultura. Dirección General de Minas, Geología e Hidrología, Buenos Aires.

Guzmán, C., E. Cristallini, and G. Bottesi (2007), Contemporary stress orientations in the Andean retroarc between 34°S and 39°S from borehole breakout analysis, *Tectonics*, *26*, Not available, doi: 10.1029/2006tc001958.

Hain, M. P., M. R. Strecker, B. Bookhagen, R. N. Alonso, H. Pingel, and A. K. Schmitt (2011), Neogene to Quaternary broken foreland formation and sedimentation dynamics in the Andes of NW Argentina (25°S), *Tectonics*, *30*, Not available, doi: 10.1029/2010TC002703.

Hallet, B., and J. Putkonen (1994), Surface dating of dynamic landforms: young boulders on aging moraines, *Science*, *265*(5174), 937–940, doi: 10.1126/science.265.5174.937.

Hilley, G. E., and M. R. Strecker (2005), Processes of oscillatory basin filling and excavation in a tectonically active orogen: Quebrada del Toro Basin, NW Argentina, *Geological Society of America bulletin*, *117*(7-8), 887–901, doi: 10.1130/B25602.1.

Huyghe, D., C. Bonnel, B. Nivière, B. Fasentieux, and Y. Hervouët (2015), Neogene tectonostratigraphic history of the southern Neuquén basin (39°-40°30'S, Argentina): implications for foreland basin evolution, *Basin Research*, *27*(5), 613–635, doi: 10.1111/bre.12091.

Jordan, T. E., B. L. Isacks, R. W. Allmendinger, J. A. Brewer, V. A. Ramos, and C. J. Ando (1983), Andean tectonics related to geometry of subducted Nazca plate, *Geological Society of America bulletin*, *94*(3), 341–361, doi: 10.1130/0016-7606(1983)94<341:ATRTGO>2.0.CO;2.

Kadinsky-Cade, K., R. Reilinger, and B. Isacks (1985), Surface deformation associated with the November 23, 1977, Caucete, Argentina, earthquake sequence, *Journal of Geophysical Research, [Solid Earth]*, *90*(B14), 12,691–12,700, doi: 10.1029/jb090ib14p12691.

Kahle, A. B., F. D. Palluconi, S. J. Hook, V. J. Realmuto, and G. Bothwell (1991), The advanced spaceborne thermal emission and reflectance radiometer (Aster), *International journal of imaging systems and technology*, *3*(2), 144–156, doi: 10.1002/ima.1850030210.

Kay, S. M., V. A. Ramos, C. Mpodozis, and P. Sruoga (1989), Late Paleozoic to Jurassic silicic magmatism at the Gondwana margin: Analogy to the Middle Proterozoic in North America?, *Geology*, *17*(4), 324–328, doi: 10.1130/0091-7613(1989)017<0324:LPTJSM>2.3.CO;2.

Kay, S. M., W. Matthew Burns, P. Copeland, and O. Mancilla (2006), Upper Cretaceous to Holocene magmatism and evidence for transient Miocene shallowing of the Andean subduction zone under the northern Neuquén Basin, GeoScienceWorld, doi: 10.1130/2006.2407(02).

Kozlowski, E., R. Manceda, and V. Ramos (1993), Estructura, in *Geología y recursos naturales de Mendoza*, vol. 1, pp. 253–256, Asociación Geológica Argentina, Buenos Aires.

Kraemer, P., J. Silvestro, F. Achilli, and W. Brinkworth (2011), Kinematics of a Hybrid Thick-thin-skinned Fold and Thrust Belt Recorded in Neogene Syntectonic Wedge-top Basins, Southern Central Andes Between 35° and 36°S, Malargüe, Argentina, in *Thrust Fault-Related Folding*, vol. Memoir 94, edited by McClay and J. Suppe, pp. 245–270, American Association of Petroleum Geologists, doi: 10.1306/13251340M943099.

Lal, D. (1991), Cosmic ray labeling of erosion surfaces: in situ nuclide production rates and erosion models, *Earth and planetary science letters*, *104*(2), 424–439, doi: 10.1016/0012-821X(91)90220-C.

Lanes, S. (2005), Late Triassic to Early Jurassic sedimentation in northern Neuquén Basin, Argentina: Tectosedimentary Evolution of the First Transgression, *Geologica Acta: an international earth science journal*, *3*(2), 81–106.

Langer, C. J., and S. Hartzell (1996), Rupture distribution of the 1977 western Argentina earthquake, *Physics of the Earth and Planetary Interiors*, *94*(1), 121–132, doi: 10.1016/0031-9201(95)03080-8.

Lavé, J., and J. P. Avouac (2000), Active folding of fluvial terraces across the Siwaliks Hills, Himalayas of central Nepal, *Journal of geophysical research*, *105*(B3), 5735–5770, doi: 10.1029/1999jb900292.

Leanza, H. A., and C. A. Hugo (2001), Hoja Geológica 3969-I Zapala.

Leland, J., M. R. Reid, D. W. Burbank, R. Finkel, and M. Caffee (1998), Incision and differential bedrock uplift along the Indus River near Nanga Parbat, Pakistan Himalaya, from 10Be and 26Al exposure age dating of bedrock straths, *Earth and planetary science letters*, *154*(1), 93–107, doi: 10.1016/S0012-821X(97)00171-4.

Lifton, N. A., J. W. Bieber, J. M. Clem, M. L. Duldig, P. Evenson, J. E. Humble, and R. Pyle (2005), Addressing solar modulation and long-term uncertainties in scaling secondary cosmic rays for in situ cosmogenic nuclide applications, *Earth and planetary science letters*, *239*(1),

140–161, doi: 10.1016/j.epsl.2005.07.001.

Lisiecki, L. E., and M. E. Raymo (2005), A Pliocene-Pleistocene stack of 57 globally distributed benthic $\delta^{18}O$ records, *Paleoceanography*, *20*(1), Not available, doi: 10.1029/2004pa001071.

Lopasso, A. M., F. Tapia, R. Feal, R. Ondrak, J. Sláma, J. Hlebszevitsch, L. Giambiagi, and M. C. Ghiglione (2024), Pleistocene deformation of the Malargüe fold–thrust belt from structural modelling and geochronology of syntectonic sedimentation, *Journal of the Geological Society*, *181*, Not available, doi: 10.1144/jgs2023-065.

López Ordines, M. A., L. Ciancio, E. A. Rojas Vera, and R. G. López (2022), Structural development in the frontal Malargüe fold and thrust belt, Neuquén Basin, Argentina, in *Andean Structural Styles*, vol. Not available, pp. 423–431, Elsevier, doi: 10.1016/b978-0-323-85175-6.00033-x.

Manceda, R., and D. Figueroa (1995), Inversion of the Mesozoic Neuquén rift in the Malargüe fold and thrust belt, Mendoza, Argentina, in *Petroleum Basins of South America*, vol. Memoir 62, edited by R. S. S. . H. J. W. A. J. Tankard, pp. 369–382, AAPG Special Volumes.

Markham, B. L., W. C. Boncyk, D. L. Helder, and J. L. Barker (1997), Landsat-7 Enhanced Thematic Mapper Plus Radiometric Calibration, *Canadian Journal of Remote Sensing*, *23*(4), 318–332, doi: 10.1080/07038992.1997.10855218.

Martinod, J., L. Husson, P. Roperch, B. Guillaume, and N. Espurt (2010), Horizontal subduction zones, convergence velocity and the building of the Andes, *Earth and planetary science letters*, *299*(3), 299–309, doi: 10.1016/j.epsl.2010.09.010.

Mescua, J. F., L. B. Giambiagi, A. Tassara, M. Gimenez, and V. A. Ramos (2014), Influence of pre-Andean history over Cenozoic foreland deformation: Structural styles in the Malargüe fold-and-thrust belt at 35°S, Andes of Argentina, *Geosphere*, *10*(3), 585–609, doi: 10.1130/GES00939.1.

Mescua, J. F., M. Barrionuevo, L. Giambiagi, J. Suriano, S. Spagnotto, E. Stahlschmidt, H. de la Cal, J. L. Soto, and M. Mazzitelli (2019), Stress field and active faults in the orogenic front of the Andes in the Malargüe fold-and-thrust belt (35°–36°S), *Tectonophysics*, *766*, 179–193, doi: 10.1016/j.tecto.2019.06.003.

Messager, G., B. Nivière, J. Martinod, P. Lacan, and J.-P. Xavier (2010), Geomorphic evidence for Plio-Quaternary compression in the Andean foothills of the southern Neuquén Basin, Argentina, *Tectonics*, *29*(4), doi: 10.1029/2009TC002609.

Messager, G., B. Nivière, P. Lacan, Y. Hervouët, and J.-P. Xavier (2014), Plio-Quaternary thin-skinned tectonics along the crustal front flexure of the southern Central Andes: a record of the regional stress regime or of local tectonic-driven gravitational processes?, *International Journal of Earth Sciences*, *103*(3), 929–951, doi: 10.1007/s00531-013-0983-4.

Messager, G., D. Huyghe, C. Bonnel, B. Nivière, and B. Fasentieux (2023), The Neogene to Quaternary evolution of the Neuquén Andes broken foreland forced by tectonic, climatic and surface processes (southern Central Andes), *Journal of South American Earth Sciences*, *131*, 104,620, doi: 10.1016/j.jsames.2023.104620.

Nivière, B., G. Messager, S. Carretier, and P. Lacan (2013), Geomorphic expression of the southern Central Andes forebulge (37°S, Argentina), *Terra nova*, *25*(5), 361–367, doi: 10.1111/ter.12044.

Nullo, F., G. Stephens, A. Combina, L. Dimieri, P. Baldauf, and P. Bouza (2004), Descripción geológica de la Hoja Malargüe Provincia de Mendoza, *Tech. rep.*, SEGEMAR.

Olivar, J., S. Nacif, M. Giménez, B. Heit, L. Fennell, and A. Folguera (2023), Structure and seismogenic activity of the broken foreland to the south of the Chilean-Pampean flat subduction zone: The San Rafael Block, *Journal of South American Earth Sciences*, *124*, 104,260, doi: 10.1016/j.jsames.2023.104260.

Oro, A., P. A. Blanc, B. Colavitto, C. Rivas, L. M. Rothis, H. N. Vargas, and L. P. Perucca (2023), Surface Deformation and Secondary Effects of the January 18th, 2021 (Mw 6.4) San Juan (Argentina) Earthquake from Remote Sensing Techniques, *Geologische Rundschau: Zeitschrift fur allgemeine Geologie*, *112*(8), 2267–2291, doi: 10.1007/s00531-023-02354-x.

Pardo, M., D. Comte, and T. Monfret (2002), Seismotectonic and stress distribution in the central Chile subduction zone, *Journal of South American Earth Sciences*, *15*(1), 11–22, doi: 10.1016/S0895-9811(02)00003-2.

Pardo-Casas, F., and P. Molnar (1987), Relative motion of the Nazca (Farallon) and South American Plates since Late Cretaceous time, *Tectonics*, *6*(3), 233–248, doi: 10.1029/TC006i003p00233.

Pepin, E., S. Carretier, G. Hérail, V. Regard, R. Charrier, M. Farías, V. García, and L. Giambiagi (2013), Pleistocene landscape entrenchment: a geomorphological mountain to foreland field case, the Las Tunas system, Argentina, *Basin Research*, *25*(6), 613–637, doi: 10.1111/bre.12019.

Polanski, J. (1962), Estratigrafía, neotectónica y geomorfología del Pleistoceno pedemontano entre los ríos Diamente y Mendoza, provincia de mendoza, *Revista de la Asociación Geológica Argentina*, *17*(3-4).

Portenga, E. W., and P. R. Bierman (2011), Understanding Earth's eroding surface with 10Be, *GSA today: a publication of the Geological Society of America*, *21*, 4–10, doi: 10.1130/G111A.1.

Ramos, V. A. (1981), Descripción geológica de la Hoja 33c, Los Chihuidos Norte, Provincia del Neuquén, *Tech. rep.*, Servicio Geológico Nacional, Buenos Aires.

Ramos, V. A. (1988), The tectonics of the Central Andes; 30° to 33° S latitude, in *Processes in Continental Lithospheric Deformation*, vol. 218, edited by S. P. Clark, pp. 31–54, Geological Society of America, doi: 10.1130/SPE218-p31.

Ramos, V. A. (1994), Terranes of Southern Gondwanaland and Their Control in the Andean Structure (30°–33°S Latitude), in *Tectonics of the Southern Central Andes: Structure and Evolution of an Active Continental Margin*, vol. Not available, edited by K.-J. Reutter, E. Scheuber, and P. J. Wigger, pp. 249–261, Springer Berlin Heidelberg, Berlin, Heidelberg, doi: 10.1007/978-3-642-77353-2_18.

Ramos, V. A., and S. M. Kay (2006), Overview of the tectonic evolution of the southern Central Andes of Mendoza and Neuquén (35°–39°S latitude), in *Evolution of an Andean Margin: A Tectonic and Magmatic View from the Andes to the Neuque´n Basin (35°-39°S lat)*, vol. Special paper 407, edited by Kay, p. 342, Geological Society of America, doi: 10.1130/2006.2407(01).

Ramos, V. A., M. Cegarra, and E. Cristallini (1996), Cenozoic tectonics of the High Andes of west-central Argentina (30–36°S latitude), *Tectonophysics*, *259*(1), 185–200, doi: 10.1016/0040-1951(95)00064-X.

Ramos, V. A., M. Escayola, D. I. Mutti, and G. I.

Vujovich (2000), Proterozoic-early Paleozoic ophiolites of the Andean basement of southern South America, in *Ophiolites and oceanic crust: new insights from field studies and the Ocean Drilling Program*, vol. Special Paper 349, edited by Dilek, pp. 331–349, Geological Society of America, doi: 10.1130/0-8137-2349-3.331.

Ramos, V. A., E. O. Cristallini, and D. J. Pérez (2002), The Pampean flat-slab of the Central Andes, *Journal of South American Earth Sciences*, *15*(1), 59–78, doi: 10.1016/S0895-9811(02)00006-8.

Regard, V., O. Bellier, J.-C. Thomas, D. Bourlès, S. Bonnet, M. R. Abbassi, R. Braucher, J. Mercier, E. Shabanian, S. Soleymani, and K. Feghhi (2005), Cumulative right-lateral fault slip rate across the Zagros—Makran transfer zone: role of the Minab—Zendan fault system in accommodating Arabia—Eurasia convergence in southeast Iran, *Geophysical Journal International*, *162*(1), 177–203, doi: 10.1111/j.1365-246X.2005.02558.x.

Regnier, M., J. L. Chatelain, R. Smalley, Jr, J.-M. Chiu, B. L. Isacks, and M. Araujo (1992), Seismotectonics of Sierra Pie de Palo, a basement block uplift in the Andean foreland of Argentina, *Bulletin of the Seismological Society of America*, *82*(6), 2549–2571, doi: 10.1785/BSSA0820062549.

Ritz, J. F., E. T. Brown, D. L. Bourlès, H. Philip, A. Schlupp, G. M. Raisbeck, F. Yiou, and B. Enkhtuvshin (1995), Slip rates along active faults estimated with cosmic-ray–exposure dates: Application to the Bogd fault, Gobi-Altaï, Mongolia, *Geology*, *23*(11), 1019–1022, doi: 10.1130/0091-7613(1995)023<1019:SRAAFE>2.3.CO;2.

Rockwell, T. K., D. E. Ragona, A. J. Meigs, L. A. Owen, C. H. Costa, and E. A. Ahumada (2014), Inferring a Thrust-Related Earthquake History from Secondary Faulting: A Long Rupture Record of La Laja Fault, San Juan, Argentina, *Bulletin of the Seismological Society of America*, *104*(1), 269–284, doi: 10.1785/0120110080.

Rockwell, T. K., C. H. Costa, A. J. Meigs, D. Ragona, L. A. Owen, M. K. Murari, E. Masana, and A. D. Richard (2022), Paleoseismology of the Marquesado-La Rinconada thrust system, Eastern Precordillera of Argentina, *Frontiers of Earth Science in China*, *10*, 1032,357, doi: 10.3389/feart.2022.1032357.

Rojas Vera, E. A., J. Mescua, A. Folguera, T. P. Becker, L. Sagripanti, L. Fennell, D. Orts, and V. A. Ramos (2015), Evolution of the Chos Malal and Agrio fold and thrust belts, Andes of Neuquén: Insights from structural analysis and apatite fission track dating, *Journal of South American Earth Sciences*, *64*, 418–433, doi: 10.1016/j.jsames.2015.10.001.

Rothis, L. M., L. P. Perucca, P. Santi Malnis, J. M. Alcacer, F. M. Haro, and H. N. Vargas (2019), Neotectonic, morphotectonic and paleoseismologic analysis of the Las Chacras Fault System, Sierras Pampeanas Occidentales, San Juan, Argentina, *Journal of South American Earth Sciences*, *91*, 144–153, doi: 10.1016/j.jsames.2019.02.001.

Schmidt, S., R. Hetzel, F. Mingorance, and V. A. Ramos (2011), Coseismic displacements and Holocene slip rates for two active thrust faults at the mountain front of the Andean Precordillera (∼33°S), *Tectonics*, *30*(5), Not available, doi: 10.1029/2011TC002932.

Siame, L. L., R. Braucher, and D. L. Bourles (2000), Les nucleides cosmogeniques produits in-situ; de nouveaux outils en geomorphologie quantitative, *Bulletin de la Société Géologique de France*, *171*(4), 383–396, doi: 10.2113/171.4.383.

Siame, L. L., O. Bellier, M. Sébrier, D. L. Bourlès, P. Leturmy, M. Perez, and M. Araujo (2002), Seismic hazard reappraisal from combined structural geology, geomorphology and cosmic ray exposure dating analyses: the Eastern Precordillera thrust system (NW Argentina), *Geophysical Journal International*, *150*(1), 241–260, doi: 10.1046/j.1365-246X.2002.01701.x.

Siame, L. L., M. Sébrier, O. Bellier, D. Bourlès, C. Costa, E. A. Ahumada, C. E. Gardini, and H. Cisneros (2015), Active basement uplift of Sierra Pie de Palo (Northwestern Argentina): Rates and inception from ^{10}Be cosmogenic nuclide concentrations, *Tectonics*, *34*(6), 1129–1153, doi: 10.1002/2014TC003771.

Silvestro, J., P. Kraemer, F. Achilli, and W. Brinkworth (2005), Evolución de las cuencas sinorogénicas de la Cordillera Principal entre 35°- 36° S, Malargüe, *Revista de la Asociación Geológica argentina*, *60*(4), 627–643.

Simoes, M., J. P. Avouac, and Y. Chen (2007), Slip rates on the Chelungpu and Chushiang thrust faults inferred from a deformed strath terrace along the Dungpuna river, west central Taiwan, *Journal of Geophysical Research, [Solid Earth]*, *112*, B03S10, doi: 10.1029/2005JB004200.

Snyder, D. B., V. A. Ramos, and R. W. Allmendinger (1990), Thick-skinned deformation observed on deep seismic reflection profiles in western Argentina, *Tectonics*, *9*(4), 773–788, doi: 10.1029/TC009i004p00773.

Soler, P., and M. G. Bonhomme (1990), Relation of magmatic activity to plate dynamics in central Peru from Late Cretaceous to present, in *Plutonism from Antarctica to Alaska*, vol. Not available, pp. 173–192, Geological Society of America, doi: 10.1130/SPE241-p173.

Somoza, R. (1998), Updated azca (Farallon)—South America relative motions during the last 40 My: implications for mountain building in the central Andean region, *Journal of South American Earth Sciences*, *11*(3), 211–215, doi: 10.1016/s0895-9811(98)00012-1.

Soria, M. (1984), Vertebrados fósiles y edad de la Formación Aisol, provincia de Mendoza, *Revista de la Asociación Geológica Argentina*, *38*(3-4), 299–306.

Sruoga, P., M. P. Etcheverría, A. Folguera, D. Repol, J. C. M. Zanettini, and L. E. Fauqué (2005), Hoja Geológica 3569-I Volcán Maipo.

Steinmann, G. (1929), Geologie von Peru, Ph.D. thesis, Carl Winters Univ. Buchhandlung, Heidelberg, Germany.

Stone, J. O. (2000), Air pressure and cosmogenic isotope production, *Journal of Geophysical Research, [Solid Earth]*, *105*(B10), 23,753–23,759, doi: 10.1029/2000JB900181.

Strecker, M. R., G. E. Hilley, B. Bookhagen, and E. R. Sobel (2012), Structural, geomorphic, and depositional characteristics of contiguous and broken foreland basins: Examples from the Eastern flanks of the central Andes in Bolivia and NW Argentina, in *Tectonics of Sedimentary Basins*, vol. Not available, pp. 508–521, John Wiley & Sons, Ltd, Chichester, UK, doi: 10.1002/9781444347166.ch25.

Uliana, M. A., K. T. Biddle, and J. Cerdan (1989), Mesozoic extension and the formation of Argentine sedimentary basins, in *Extensional Tectonics and Stratigraphy of the North Atlantic Margins*, edited by Tankard, chap. 39, pp. 599–614, AAPG Special Volumes.

Vergani, G. D., A. J. Tankard, H. J. Belotti, and H. J. Welsink (1995), Tectonic evolution and paleogeography of the Neuquén Basin, Argentina, in *Petroleum Basins of South*

America, vol. Memoir 62, edited by A. J. Tankard and H. J. Welsink, AAPG Special Volumes.

Volkheimer, W. (1978), Descripción Geológica de la Hoja 27b, Cerro Sosneado, *Tech. rep.*, Servicio Geológico Nacional.

von Gosen, W. (1998), Transpressive deformation in the southwestern part of the Sierra de San Luis (Sierras Pampeanas, Argentina), *Journal of South American Earth Sciences*, *11*(3), 233–264, doi: 10.1016/S0895-9811(98)00013-3.

Zapata, T. R., and R. W. Allmendinger (1996), Growth stratal records of instantaneous and progressive limb rotation in the Precordillera thrust belt and Bermejo basin, Argentina, *Tectonics*, *15*(5), 1065–1083, doi: 10.1029/96TC00431.

Zöllner, W., and A. J. Amos (1973), Descripción geológica de la hoja 32b, Chos Malal, *Tech. rep.*, Servicio Geológico Nacional Argentino, Buenos Aires.